J. Fluid Mech. (2003), *vol.* 479, *pp.* 65–98.
DOI: 10.1017/S0022112002003312 Printed in the United Kingdom

The effect of surface tension on rimming flows in a partially filled rotating cylinder

By J. ASHMORE[1], A. E. HOSOI[2]† AND H. A. STONE[1]

[1]Division of Engineering and Applied Sciences, Harvard University, Cambridge, MA 02138, USA

[2]Department of Mathematics, Harvey Mudd College, Claremont, CA 91711, USA

(Received 30 May 2001 and in revised form 19 September 2002)

We study the shape of the interface in a partially filled horizontal cylinder which is rotating about its axis. Two-dimensional steady solutions for the interface height are examined under the assumptions that the filling fraction is small, inertia may be neglected, and the fluid forms a continuous film covering the surface. Three different regimes of steady solutions have been reported in the literature, corresponding to limits in which the ratio of gravitational to viscous forces (as defined in the text) is small, moderate or large. In each case, solutions have only been described analytically in the limit that surface tension effects are negligible everywhere. We use analytical and numerical methods, include surface tension and study steady solutions in a regime when the ratio of gravitational to viscous forces is large. This solution comprises a fluid pool that sits near the bottom of the cylinder and a film that coats the sides and top of the cylinder, the thickness of which can be determined by Landau–Levich–Derjaguin type arguments. We also examine the effect of surface tension on the solutions in the limits of the ratio of gravity to viscous forces being moderate and small.

1. Introduction

The coating of moving substrates arises in many industrial applications owing to the need to control, protect and functionalize surfaces. The subject provides entry into a number of different fluid mechanical problems involving free boundaries. We address one problem in this class: the coating of a Newtonian fluid on the interior of a steadily rotating horizontal cylinder. Previous analytical and numerical studies have, for the most part, neglected the influence of surface tension, as we summarize below. Here we emphasize the role of surface tension and provide both analytical and numerical results illustrating the connection with the Landau–Levich–Derjaguin class of problems.

Much work associated with coating horizontal rotating cylinders was initiated by Moffatt (1977), who investigated the shape of the thin film that completely coats the outside of a horizontal rotating cylinder. Experimental and numerical work on the interface shape of a continuous film coating the interior of a rotating cylinder has described many interesting effects, including three-dimensional instabilities and time-periodic flows (Balmer 1970; Hosoi & Mahadevan 1999; Karweit & Corrsin 1975; Melo 1993; Thoroddsen & Mahadevan 1997). Two-dimensional (axially uniform) steady states are also observed experimentally, and analytical studies have been

† Present address: Department of Mechanical Engineering, MIT, Cambridge, MA 02139, USA.

	$A^2\rho gR/\mu\Omega \lesssim 2$ (nearly uniform film)	$2 \lesssim A^2\rho gR/\mu\Omega \lesssim 5$ (accumulation of fluid on rising side of cylinder)	$A^2\rho gR/\mu\Omega \gtrsim 5$ (thin film pulled out from pool in bottom)
Zero surface tension	Ruschak & Scriven (1976) (A)	Benjamin *et al.* (1993) (A,N) Johnson (1988) (A,N) Moffatt (1977) (A) O'Brien & Gath (1988) (A) Ruschak & Scriven (1976) (A,N) Tirumkudulu & Acrivos (2001) (A,N) Wilson & Williams (1997) (N)	Tirumkudulu & Acrivos (2001) (A,N)
Non-zero surface tension	Benjamin *et al.* (1993) (E) Ruschak & Scriven (1976) (A) Orr & Scriven (1978) (N) Rajagopalan *et al.* (1992) (A,N) This paper (A,N)	Benjamin *et al.* (1993) (E) Thoroddsen & Mahadevan (1997) (E) Tirumkudulu & Acrivos (2001) (N,E) Hosoi & Mahadevan (1999) (A,N) Melo (1993) (E) Wilson & Williams (1997) (N) This paper (A,N)	Benjamin *et al.* (1993) (E) Thoroddsen & Mahadevan (1997) (E) Tirumkudulu & Acrivos (2001) (A,N,E) This paper (A,N)

TABLE 1. A characterization of the parameter regimes previously studied for two-dimensional steady flow, and those studied in this paper. A denotes analytical work, N numerical work and E experimental work.

restricted to these (Johnson 1988; Moffatt 1977; O'Brien & Gath 1988; Ruschak & Scriven 1976), with the exception of unpublished work by Benjamin, Pritchard & Tavener (1993). Research in this area has overlapped work on coating the outside of a rotating cylinder, which is similar in certain regions of parameter space (Duffy & Wilson 1999; Hansen & Kelmanson 1994; Hinch & Kelmanson 2002; Kelmanson 1995; Peterson, Jimack & Kelmanson 2001; Preziosi & Joseph 1988; Pukhnachev 1977).

For coating flows inside a rotating horizontal cylinder, previous analytical studies of two-dimensional steady-state solutions describing the interface height have focused on limits in which surface tension is negligible (table 1). Since the complete lubrication equation for the interface height is a third-order nonlinear differential equation in which the surface tension effects represent a singular perturbation, we expect that surface tension may have a significant effect on the qualitative and quantitative behaviours of the system, at least in some regions of parameter space. We present a combination of analytical and numerical results that describe solutions within and outside the restricted parameter range studied previously, and which account for the effect of surface tension.

We measure the ratio of the gravitational to the viscous forces by the dimensionless parameter $\lambda = A^2\rho gR/\mu\Omega$ where A is the filling fraction of fluid inside the cylinder, ρ is the density, g is the gravitational constant, R is the radius of the cylinder, μ is the viscosity, and Ω is the rotation rate. Qualitatively different solutions have

been reported in the literature in the three regions $0 < \lambda \lesssim 2$ ('fast' rotation), $2 \lesssim \lambda \lesssim 5$ ('moderate' rotation) and $\lambda \gtrsim 5$ ('slow' rotation). In each case, there are also restrictions on the value of the Bond number $\mathscr{B} = \rho g R^2/A\gamma$ for surface tension effects (γ) to be negligible.

Most theoretical work has utilized lubrication theory, valid when the filling fraction $A \ll 1$. Although the full lubrication equation is a third-order ordinary differential equation, it has been common for researchers to study a truncated equation in which only two viscous terms and one gravitational term are retained, and all surface tension terms are neglected. Only the neglected terms involve derivatives and the truncated equation is algebraic. The solutions to the truncated equation are accurate provided the gradients do not become large so that the neglected terms which involve derivatives are always small, which is true when $\lambda < 2$. The truncated algebraic equation yields discontinuous solutions when $2 \lesssim \lambda \lesssim 5$ and no solutions when $\lambda \gtrsim 5$. Tirumkudulu & Acrivos (2001) recognized that including the most significant extra gravity term, which involves the first derivative of the interface height, results in a continuous solution for all λ (see equation (2.13) and related discussion). In this paper we include the influence of the surface tension term and study regimes where the effect of surface tension modifies the continuous solution found by Tirumkudulu & Acrivos (2001).

We show that the inclusion of surface tension may be particularly significant in the limit $\lambda \gtrsim 5$. Qualitatively, in this limit the solution always has the appearance of a pool of fluid lying in the bottom of the cylinder with a thin, almost uniform, film coating the sides and top. In the solution found by Tirumkudulu & Acrivos (2001), surface tension is entirely negligible and the dimensional film thickness scales as $(\mu\Omega R)^{1/2}A^{-1/6}(\rho g)^{-1/2}$. In this paper we describe quantitatively different solutions in which surface tension forces are important in setting the thickness of the film that coats the sides and top of the cylinder. Physically, the large curvature where the film is extracted from the pool leads to a capillary pressure gradient that restricts the fluid flux in the film. The detailed analysis leads to a prediction of film thickness which scales as $(\mu\Omega R)^{2/3}A^{-1/3}\gamma^{-1/6}(\rho g)^{-1/2}$ or $(\mu\Omega)^{2/3}R^{7/15}\gamma^{-1/15}(\rho g)^{-3/5}A^{-2/5}$, depending on the geometry. Once the role of surface tension and geometry are recognized, the analysis is similar to that of Landau & Levich (1942) and Derjaguin (1943) who described the thickness of the fluid film deposited on a plate or cylinder withdrawn from a bath at constant velocity. Whereas the results of Tirumkudulu & Acrivos (2001) are valid at high effective capillary numbers, defined in the main text, our results are valid at low effective capillary numbers.

In the limit $2 \lesssim \lambda \lesssim 5$, when viscous and gravitational forces are of the same order of magnitude, discontinuous solutions arise when the 'extra' gravitational and surface tension terms are neglected (see equation (2.13) below). Tirumkudulu & Acrivos (2001) showed that solutions are continuous when the most important extra gravitational term is included. We include both the most important extra gravitational terms and surface tension and consider the effect of surface tension on the solution. Finally, when $0 < \lambda \lesssim 2$ and viscous forces dominate gravitational forces, surface tension has little effect.

We consider only axially uniform (two-dimensional) solutions, although there are regions in which the two-dimensional steady solutions are not stable and instead the physical solution is three-dimensional, time-periodic or even chaotic. Many such states were documented by Benjamin *et al.* (1993) and Thoroddsen & Mahadevan (1997) and others. However, each of the solutions we present is observed in certain regions of parameter space and we comment on this in § 5.

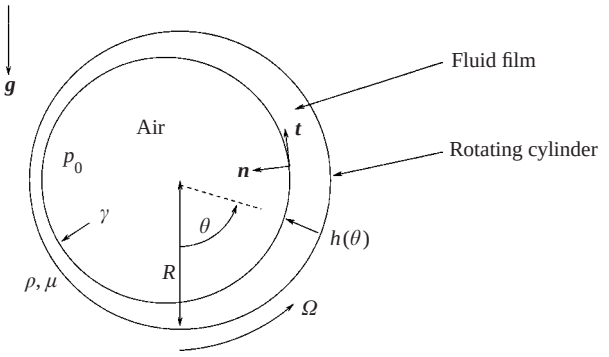

FIGURE 1. Thin-film flow inside a rotating horizontal cylinder.

The second section describes a lubrication model and derives the equation for the interface height. In §§3 and 4 we present and discuss our results for the two cases when surface tension effects are significant, $\lambda \gtrsim 5$ and $2 \lesssim \lambda \lesssim 5$. Owing to the nonlinearity of the interface-shape equation, it has not been possible to obtain analytical solutions in all cases. However, we are able to find asymptotic scaling results instead. In §5 we discuss our results, their stability, and present our conclusions. Four appendices include basic details of the analysis, and provide comparisons with existing research. Appendix A contains the derivation of the flow equations and Appendix B a description of the numerical methods used. We discuss some details of the slow-rotation solution described by Tirumkudulu & Acrivos (2001) in Appendix C, and in Appendix D we include a comparison between numerical results and the theoretical results established by Ruschak & Scriven (1976) for the case $\lambda \lesssim 2$.

2. Model

We consider the film shape inside a partially filled, horizontal rotating cylinder. Our focus is on thin films so that a lubrication analysis is valid, and we restrict our attention to steady two-dimensional solutions, including the influence of surface tension. We use a plane polar coordinate system (r, θ) with origin at the centre of the cylinder and measure θ in the sense of rotation with $\theta = 0$ coinciding with the downward vertical (figure 1). The radius of the cylinder is denoted by R, the filling fraction by A, the rotation rate by Ω, and the interface height $h(\theta)$ where $r = R - h(\theta)$. The fluid has density ρ, viscosity μ and surface tension γ. Throughout the discussion below we assume that the film remains continuous.

As our interest concerns steady shapes, the fluid motion is described by the two-dimensional time-independent Navier–Stokes equations for an incompressible flow

$$\nabla \cdot \boldsymbol{u} = 0, \tag{2.1a}$$

$$\rho \boldsymbol{u} \cdot \nabla \boldsymbol{u} = -\nabla p + \mu \nabla^2 \boldsymbol{u} + \rho \boldsymbol{g}, \tag{2.1b}$$

where $\boldsymbol{u}$ is the velocity vector, p is the pressure and $\boldsymbol{g}$ is the force per unit mass due to gravity. We require the 2π-periodic solutions to satisfy the boundary conditions

$$\boldsymbol{u} = \Omega R \boldsymbol{e}_\theta \qquad \text{at } r = R, \tag{2.2a}$$

$$\boldsymbol{n} \cdot \boldsymbol{T} + p_0 \boldsymbol{n} = \gamma \kappa \boldsymbol{n} \qquad \text{at } r = R - h(\theta), \tag{2.2b}$$

where $\boldsymbol{T}$ is the stress tensor, $\boldsymbol{n}$ is the unit normal vector to the interface directed away from the fluid, p_0 is the constant pressure inside the cylinder, and κ is the curvature

of the free surface. By definition of the filling fraction A, we also require the solution to satisfy the integral condition

$$\int_0^{2\pi} \left[h(\theta) - \frac{h(\theta)^2}{2R} \right] \mathrm{d}\theta = \pi R A. \tag{2.3}$$

2.1. *Non-dimensionalization*

We shall assume that the filling fraction is small $A \ll 1$, so that the film thickness and its variations are expected to be small everywhere (as is verified after obtaining the solution), and hence we utilize a lubrication approximation. Then, denoting dimensionless variables with a tilde, we non-dimensionalize according to:

$$\left.\begin{aligned} u_\theta = \Omega R \tilde{u}_\theta, \quad u_r = A\Omega R \tilde{u}_r, \quad r = R(1 - A\tilde{r}), \\ h(\theta) = AR\tilde{h}(\theta), \quad p = \frac{\mu\Omega}{A^2}\tilde{p}, \quad \kappa = \frac{A}{R}\tilde{\kappa}. \end{aligned}\right\} \tag{2.4}$$

Now, $\tilde{r} = 0$ denotes the cylinder surface. Note that we have scaled the interface curvature as $O(A/R)$ since for nearly uniform films this is the magnitude of the curvature variations that establish a capillary pressure gradient.

There are four independent non-dimensional parameters. The first two are the Reynolds number $\mathscr{R} = \rho\Omega R^2/\mu$ and the filling fraction A. The remaining two are a gravitational parameter λ and the Bond number $\mathscr{B}$, here defined as

$$\lambda = \frac{A^2 \rho g R}{\mu\Omega}, \qquad \mathscr{B} = \frac{\rho g R^2}{A\gamma}, \tag{2.5}$$

representing, respectively, the ratio of gravitational to viscous forces, and the ratio of gravitational to surface tension forces. Note that the product $\mathscr{B}/\lambda = \mu\Omega R\gamma^{-1}A^{-3}$ is a capillary number, representing the ratio of viscous to surface tension stresses, and naturally appears when studying the influence of interfacial tension on free-surface shapes as we do here.

The relationship between the three independent parameters we use to characterize solutions, A, λ and $\mathscr{B}$, and the parameters F, α, β and $\mathscr{C}$ used in the recent paper by Tirumkudulu & Acrivos (2001) is $F = A$, $\alpha = A/\sqrt{\lambda}$, $\beta = \sqrt{\lambda}$ and $\mathscr{C} = \mu\Omega R/\gamma = A^3\mathscr{B}/\lambda$. We shall sometimes rewrite results in this notation to aid the reader.

In addition to the filling fraction being small, $A \ll 1$, we assume the Reynolds number is not too large in the sense that $A^2\mathscr{R} \ll 1$, as is characteristic of many lubrication analyses. The full dimensionless equations are given in Appendix A. Performing an expansion using lubrication theory with the small parameter A, we retain viscous terms $O(A)$, gravitational terms $O(A\lambda)$ and surface tension terms $O(A\lambda\mathscr{B}^{-1})$. This approach will enable us to consider a range of values of the gravitational parameter λ. Then the dimensionless continuity and momentum equations, with tildes dropped, are

$$-(1 - Ar)\frac{\partial u_r}{\partial r} + Au_r + \frac{\partial u_\theta}{\partial \theta} + O(A^2) = 0, \tag{2.6a}$$

$$\frac{\partial p}{\partial r} + A\lambda\cos\theta + O(A^2,\ A^3\mathscr{R}) = 0, \tag{2.6b}$$

$$-(1 + Ar)\frac{\partial p}{\partial \theta} + \frac{\partial^2 u_\theta}{\partial r^2} - A\frac{\partial u_\theta}{\partial r} - \lambda\sin\theta + O(A^2,\ A^2\mathscr{R}) = 0, \tag{2.6c}$$

subject to the boundary conditions

$$\boldsymbol{u} = \boldsymbol{e}_\theta \qquad \text{at } r = 0 \qquad \text{(no-slip velocity condition)} \qquad (2.7a)$$

$$\frac{\partial u_\theta}{\partial r} + Au_\theta + O(A^2) = 0 \qquad \text{at } r = h(\theta) \qquad \text{(tangential stress condition)} \qquad (2.7b)$$

$$p = p_0 - \lambda \mathscr{B}^{-1}\kappa + O(A^2) \qquad \text{at } r = h(\theta) \qquad \text{(normal stress condition)} \qquad (2.7c)$$

$$\int_0^{2\pi} \left[h(\theta) - \frac{Ah(\theta)^2}{2}\right] \mathrm{d}\theta = \pi \qquad \text{(integral condition).} \qquad (2.7d)$$

Owing to the complicated nature of this free-boundary problem, the lubrication approximation has been utilized extensively, as described in many papers given in the introduction and references. Except for the unpublished work of Benjamin *et al.* (1993), the influence of surface tension has not been investigated analytically.

2.2. *Curvature approximations*

The full expression for the non-dimensional curvature κ is

$$\kappa = \frac{1}{A}\left(1 + \left(\frac{Ah'}{1-Ah}\right)^2\right)^{-3/2}\left[\left(\frac{1}{1-Ah} + \frac{Ah''}{(1-Ah)^2}\right)\left(1 + \left(\frac{Ah'}{1-Ah}\right)^2\right) + \frac{A^2h'^2}{(1-Ah)^3} - \frac{A^3h'^2h''}{(1-Ah)^4}\right], \quad (2.8)$$

where a prime denotes differentiation with respect to θ. Using only the assumption that $A \ll 1$, but allowing for the possibility that $|h'| = O(A^{-1})$, this approximates to $\kappa = 1/A + \kappa_0 + A\kappa_1 + O(A^2)$ where

$$\kappa_0 = \frac{h + h''}{(1 + (Ah')^2)^{3/2}}, \quad \kappa_1 = \frac{h^2 + 2hh'' + 2h'^2}{(1 + (Ah')^2)^{3/2}}. \qquad (2.9)$$

In general we have used both (2.8) and (2.9), which assumes $A \ll 1$, in our numerical simulations. We have had numerical difficulties using (2.8), apparently due to cancellation of terms of comparable magnitude when $A \lesssim 0.05$. Otherwise we have compared (2.8) and (2.9) and they yield the same results.

If it is also true that gradients are not too large in the sense that $|h'| \ll A^{-1}$, then a further approximation is valid: $\kappa = 1/A + (h + h'') + A(h^2 + 2hh'' + h'^2/2) + O(A^2)$. In explaining our numerical results via analytical arguments, when $|h'| \ll A^{-1}$ also we shall use the further approximation $\kappa \approx \kappa_0 = h + h'' + O(A)$. (This approximation is not made in our numerical simulations.) Note that the leading-order $1/A$ term in equation (2.8) is a constant, and as only variations of curvature lead to contributions to flow, this term does not appear in the final evolution equation for the film shape.

2.3. *Derivation of the flux equation*

We next obtain an equation for $h(\theta)$, retaining the influence of surface tension. The details of the derivation are given in Appendix A. Solving equation (2.6*b*) subject to the normal stress boundary condition (2.7*c*) yields

$$p = p_0 - \lambda \mathscr{B}^{-1}\kappa + A\lambda(h - r)\cos\theta + O(A^2, A^3\mathscr{R}, A\lambda\mathscr{B}^{-1}), \qquad (2.10)$$

where we have indicated the order of magnitude of the error to be expected, which we shall continue to do throughout this section. Substituting (2.10) into (2.6*c*) and solving for the azimuthal velocity u_θ subject to boundary conditions (2.7*a*) and (2.7*b*)

leads to

$$u_\theta(r,\theta) = 1 - \left(\lambda\sin\theta - \lambda\mathscr{B}^{-1}\frac{\mathrm{d}\kappa_0}{\mathrm{d}\theta}\right)\left(hr - \tfrac{1}{2}r^2\right)$$
$$-A\left[r - \lambda\sin\theta\left(\tfrac{1}{3}r^3 - hr^2 + \tfrac{3}{2}h^2r\right) + \lambda h'\cos\theta\left(hr - \tfrac{1}{2}r^2\right)\right.$$
$$\left. - \lambda\mathscr{B}^{-1}\frac{\mathrm{d}\kappa_0}{\mathrm{d}\theta}\left(-\tfrac{1}{3}r^3 + \tfrac{1}{2}hr^2 - \tfrac{1}{2}h^2r\right) - \lambda\mathscr{B}^{-1}\frac{\mathrm{d}\kappa_1}{\mathrm{d}\theta}\left(hr - \tfrac{1}{2}r^2\right)\right]$$
$$+O(A^2,\ A^2\mathscr{R},\ A^2\lambda,\ A^2\lambda\mathscr{B}^{-1}). \tag{2.11}$$

We integrate the continuity equation to find the constant dimensionless flux, q, defined by

$$q = \int_0^{h(\theta)} u_\theta(r,\theta)\,\mathrm{d}r, \tag{2.12}$$

corresponding to an actual flux scaled by $A\Omega R^2$. This yields the flux equation

$$q = \underbrace{h}_{\text{(I)}} \underbrace{-\tfrac{1}{3}\lambda h^3\sin\theta}_{\text{(II)}} + \underbrace{\tfrac{1}{3}\lambda\mathscr{B}^{-1}h^3\frac{\mathrm{d}\kappa_0}{\mathrm{d}\theta}}_{\text{(III)}}$$
$$-A\left[\tfrac{1}{2}h^2 - \tfrac{1}{2}\lambda h^4\sin\theta + \underbrace{\tfrac{1}{3}\lambda h^3h'\cos\theta}_{\text{(IV)}} + \tfrac{1}{6}\lambda\mathscr{B}^{-1}h^4\frac{\mathrm{d}\kappa_0}{\mathrm{d}\theta} - \tfrac{1}{6}\lambda\mathscr{B}^{-1}h^4\frac{\mathrm{d}\kappa_1}{\mathrm{d}\theta}\right]$$
$$+\,O(A^2,\ A^2\mathscr{R},\ A^2\lambda,\ A^2\lambda\mathscr{B}^{-1}), \tag{2.13}$$

where the numbered terms represent forces as follows: (I) – leading-order viscous, (II) – leading-order gravity, (III) – leading-order surface tension, (IV) – first-order gravity. This equation was previously given, in a slightly different notation, in the unpublished study by Benjamin *et al.* (1993). We note that in the curvature expressions (κ_0, κ_1) retention of the $O(A^2)$ terms which multiply h'^2 is not, strictly speaking, asymptotically consistent; nevertheless it is common to retain them since the $O(A^2)$ terms make the equation uniformly valid, even when a thin nearly uniform film connects to a deep nearly static pool (see § 3) (e.g. Wilson 1981).

We seek solutions $h(\theta)$ of equation (2.13) that are 2π-periodic and that satisfy the integral boundary condition (2.7*d*). Here, the flux q is an unknown constant which must be determined as part of the solution of the problem. The flux equation (2.13) is studied in three different regimes of parameter space: when the viscous forces are small, comparable to and large relative to the gravitational forces, corresponding to the limits $\lambda \gtrsim 5$, $2 \lesssim \lambda \lesssim 5$ and $\lambda \lesssim 2$ respectively. When both surface tension and first-order gravity are neglected, sharp transitions between qualitatively different solutions occur at the critical values $\lambda = 2.00$ and $\lambda = 4.86$, but since these transitions are smooth when equation (2.13) is solved (see also Tirumkudulu & Acrivos 2001) we use the approximate value $\lambda = 5$ to characterize the transition at $\lambda = 4.86$. Rather than numerically solving (2.13), we have instead found it more convenient to solve the time-dependent lubrication problem and evolve towards steady-state shapes $h(\theta)$, as described in Appendix B. The numerical methods used are based on those of Hosoi & Mahadevan (1999). Steady states found by this approach correspond to the solution of the time-independent problem and so yield q and $h(\theta)$. In order to quantify and

understand the numerical results, we present analytical arguments that are based on (2.13).

2.4. *Qualitative discussion*

In almost all previous theoretical and numerical studies, surface tension has been neglected ($\mathscr{B} = \infty$) and, for the case where first-order effects ($O(A)$ terms in (2.13)) are also neglected, an upper limit of $\lambda = 4.86$ has been determined; there is no steady solution $h(\theta)$ to the truncated form of (2.13) when λ exceeds this value (Benjamin *et al.* 1993). (Note that the value $\lambda = 4.86$ differs slightly from the value that derives from the critical condition given by Benjamin *et al.* 1993.) In the actual physical problem, however, when λ is greater than this value there is a steady solution and its detailed structure depends on the relative magnitude of the surface tension and gravitational terms.

Tirumkudulu & Acrivos (2001) showed that inclusion of the first-order gravity term leads to a solution when $\lambda \gtrsim 5$, which in their notation corresponds to $F/\alpha = \beta \gtrsim 2.2$. (The inclusion of first-order gravity also has important implications for the solution in the limit $2 \lesssim \lambda \lesssim 5$, which we discuss in §4.) Their solution is valid when surface tension is negligible, which leads to the restriction that an appropriately defined capillary number must be *large* (discussed further below, see table 3). We find numerically that when surface tension is significant ($\mathscr{B}$ finite) two distinct steady solutions also exist when appropriately defined capillary numbers are *small*, and the film thickness scales with rotation rate and material parameters in a quantitatively different manner than obtained by Tirumkudulu & Acrivos (2001), even though the solutions are qualitatively similar, i.e. there is a pool at the bottom of the cylinder with thin films on either side. There is still likely to be an upper limit to λ corresponding to the film becoming so thin that it is unstable and dewets, but this limit is beyond the goal of the study presented here.

The order of magnitude of the gravitational parameter λ is particularly important in determining the qualitative behaviour of the system. To illustrate this point, we show in figure 2 the results of numerical simulations of (2.13) for λ ranging between 1 and 50. In all cases the Bond number $\mathscr{B} = 100$ and filling fraction $A = 0.1$. The film varies from a nearly uniform thickness characteristic of higher rotation speeds (λ small) to highly non-uniform shapes that exhibit sharp gradients at lower rotation speeds (λ large).

As a first set of comments we indicate some qualitative ideas that are important in characterizing the solutions. When the value of the gravitational parameter $\lambda \gtrsim 5$ and surface tension and/or first-order gravity effects are included, there is a steady solution comprising a pool in the bottom of the cylinder and a thin film which is pulled out by the rotating cylinder. We have identified scaling laws for both the pool and the thin film in terms of λ and the Bond number for the distinctive features of the film shape when surface tension is critical in setting the film thickness. Our results describe the scaling for two distinct subcases, depending on the ratio of the cylinder radius R to the capillary length $(\gamma/\rho g)^{1/2}$. When λ falls between two critical values, $2 \lesssim \lambda \lesssim 5$, the viscous force is strong enough to pull fluid up from the bottom of the cylinder but the gravitational force prevents the fluid from being pulled all the way over the top. Fluid accumulates in the quadrant $0 \leqslant \theta \leqslant \pi/2$, as can be seen from the $\lambda = 3$ curve in figure 2. Finally, when the value of the gravitational parameter λ is less than the smaller of the two critical values, $\lambda \lesssim 2$, the film shape is nearly uniform and the influence of surface tension is small. An analytic description of this shape in

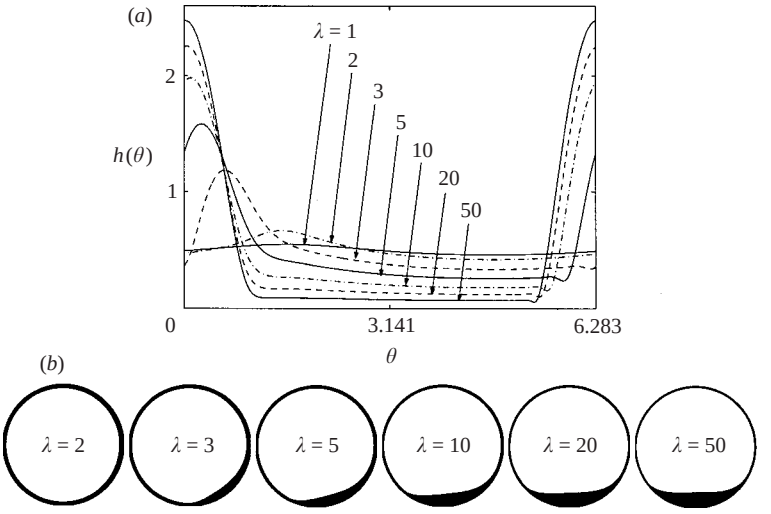

FIGURE 2. A range of solutions, showing the effect of variation of λ:(*a*) interface height plotted as a function of θ using Cartesian axes, (*b*) interface height plotted using plane polar coordinates. In all cases $\mathscr{B} = 100$, $A = 0.1$. As λ increases from small to large, we see an evolution from a nearly uniform film to a 'deep' pool at the bottom of the cylinder, which is then connected to a thin film. It is important to recognize that if surface tension and first-order gravity effects were neglected entirely then no solutions would exist for $\lambda \gtrsim 5$.

the limit $A < \lambda \ll 2$ was given by Ruschak & Scriven (1976) and is extended slightly in Appendix D.

Second, we discuss the way in which surface tension influences these different limits. If gradients do not become sufficiently large for surface tension to become important, surface tension will have little effect. This is true in two cases: (i) nearly uniform films that occur when $\lambda \ll 2$ and (ii) the solution described by Tirumkudulu & Acrivos (2001), in which a film is withdrawn from a pool of fluid in the bottom of the cylinder ($\lambda \gtrsim 5$ and large effective capillary number, see table 3). On the other hand, when solutions have large curvatures in some region, the local effect of surface tension may extend downstream and result in a quantitatively different asymptotic scaling of the interface height over a significant range of θ. This is the case for the solutions we present here, valid when $\lambda \gtrsim 5$ and effective capillary numbers, defined below in table 2, are small. Finally, when $2 \lesssim \lambda \lesssim 5$, the zero-surface-tension solution with first-order gravity effects neglected is discontinuous whereas the solution with either first-order gravity (Tirumkudulu & Acrivos 2001) or surface tension effects included (or both) is continuous. (We have demonstrated that only including surface tension leads to continuous solutions numerically.) Qualitatively, as the Bond number decreases, i.e. surface tension becomes stronger, the solutions have smaller curvatures. (The results are also summarized in tabular form in table 3.)

Having commented on the dependence of the solution on λ and Bond number, we describe the dependence on filling fraction A. For those cases where surface tension effects are most significant, the dominant balance in (2.13) for most θ is between terms (I), (II) and (III), and term (IV) is unimportant. When this is the case, the only effect of the filling fraction A on the non-dimensional solution is in setting the values of λ and the Bond number, and so it is not the actual value of the filling fraction A that is important but rather its ratio to material and geometrical parameters. (The

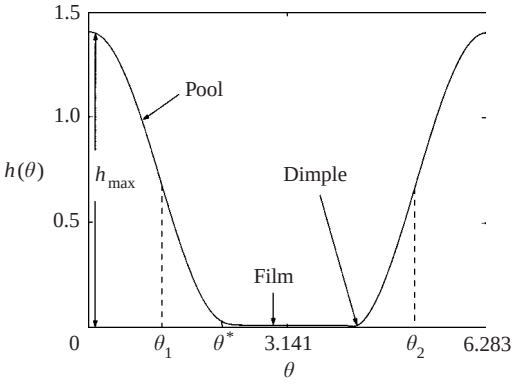

FIGURE 3. Plot of numerical solution to the full flux equation (2.13). The dimensionless solution with $\lambda = 500$, $\mathscr{B} = 1$, $A = 0.3$.

dimensional interface height has been scaled by AR and so the value of the filling fraction is important in the dimensional solution.) The first-order gravity term (IV) is sometimes important in the limit $\lambda \gtrsim 5$ when there may be a flat ('static') pool in the bottom of the cylinder, described by a balance between gravity terms (II) and (IV). We discuss this limit in § 3.1. Also in the limit $2 \lesssim \lambda \lesssim 5$, term (IV) smooths the solutions which are discontinuous when both surface tension and first-order gravity are neglected. The cases where term (IV) is important and surface tension is negligible were discussed by Tirumkudulu & Acrivos (2001).

Other researchers have typically used a different non-dimensionalization, instead scaling the dimensional film thickness by a factor of $\sqrt{\lambda}R$. In this case, if surface tension and first-order gravity effects are retained, the only parameters appearing in the flux equation are $1/\sqrt{\lambda}\mathscr{B}$ and $A/\sqrt{\lambda}$ but the integral condition (2.7d) is also dependent on λ. Although this non-dimensionalization is common, when including surface tension we have found advantageous the use of the non-dimensionalization given in (2.4), which makes the integral condition independent of λ and Bond number $\mathscr{B}$.

3. Numerical and scaling results: $\lambda \gtrsim 5$

When the cylinder is spinning sufficiently slowly, $\lambda \gtrsim 5$, and much of the fluid sits in a pool in the bottom of the cylinder, with a very small amount of fluid being pulled out into a thin film covering its sides and top. We shall describe two new solutions of this general form which arise in different regions of parameter space. Although we have not obtained an explicit analytical solution for the interface profile $h(\theta)$, asymptotic analysis and scaling arguments enable us to understand the qualitative and quantitative trends in the numerical solutions and the mechanisms that dominate. In figure 3, we show a typical numerical solution for $h(\theta)$ in the $\lambda \gtrsim 5$ limit ($A = 0.3$) and we also introduce some useful notation.

For the two solutions which we shall describe, surface tension is important in the generation of the thin film as in the Landau–Levich–Derjaguin argument (Derjaguin 1943; Landau & Levich 1942). The difference between the solutions is in the pool, which may be either almost flat or curved depending on the dominant force balance, as shown in figure 4(a,b). There are three regions of the shape profile in which the solution displays different qualitative behaviour and the dominant force balance differs; these are

Parameter balance determining pool shape ($\lambda \gtrsim 5$ for a pool)	Necessary conditions for film analysis to hold
$\mathscr{B}^{-3/5} \ll A \ll 1$	$\dfrac{A^2\mathscr{B}}{\lambda} \ll 1,\ \mathscr{B} \gg A^{-1}$
$A \ll \mathscr{B}^{-3/5} \ll 1$	$\dfrac{A^2\mathscr{B}}{\lambda} \ll A^2\mathscr{B}^{6/5} \ll 1,\ \mathscr{B} \gg A^{-1}$

TABLE 2. Conditions required for the analysis to hold in the pool and in the film regions when $\lambda \gtrsim 5$. The parameter $A^2\mathscr{B}/\lambda = \mu\Omega R/A\gamma$ is an effective capillary number. In the notation of Tirumkudulu & Acrivos (2001), the effective capillary number is $\mathscr{C}/F$.

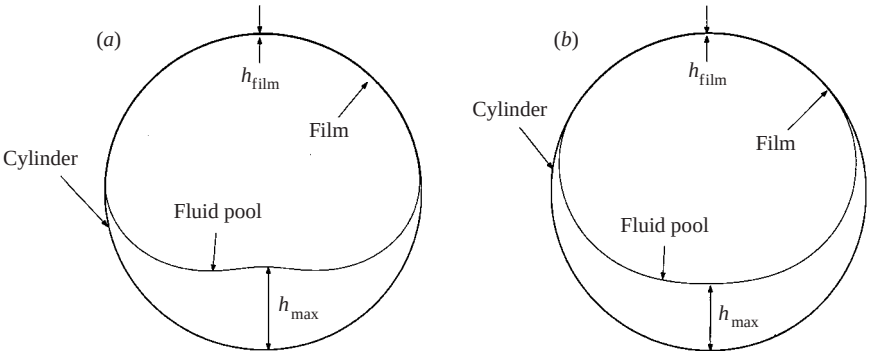

FIGURE 4. Plot of numerical solution to the full flux equation (2.13). (*a*) The dimensional solution with $\lambda = 500$, $\mathscr{B} = 5$, $A = 0.3$. (*b*) $\lambda = 500$, $\mathscr{B} = 1$, $A = 0.3$.

(i) a pool region in the bottom of the cylinder where the dominant force balance is between gravity (II) and first-order gravity (IV) or between gravity (II) and surface tension (III);

(ii) a thin film where the thickness is set by a force balance between viscous (I) and surface tension forces (III), with matching to the pool solution;

(iii) in the neighbourhood where the film re-enters the pool, there is a dimple created by a force balance between viscous (I) and surface tension forces (III).

We consider each of these regions in turn below. In §§3.1 to 3.3, we proceed by giving the dominant balances and asymptotic scalings consistent with these balances. In each case, we present numerical results that confirm the predictions and also indicate breakdown of the scaling ideas. Restrictions on the validity of each result are indicated throughout and are summarized in table 2. Finally, in §3.4 we discuss how the flux q varies as a function of λ and Bond number $\mathscr{B}$.

3.1. *The pool*

As is evident in figure 3, for $\lambda \gtrsim 5$ the film shape has a well-defined maximum near $\theta = 0$ and the pool has a well-defined width. We determine the scaling of the maximum thickness of the film in the pool, $h_{\max}$, and the width of the pool, $2\Delta\theta$, by asymptotic analysis; $\Delta\theta$ is defined as $\Delta\theta = \theta_1 - \theta_2 + 2\pi$ where numerically we take $h(\theta_1) = h(\theta_2) = h_{\max}/2$ and $0 < \theta_1 < \pi/2$, $3\pi/2 < \theta_2 < 2\pi$. The numerical results show that there is a slight asymmetry in the pool about $\theta = 0$ arising from viscous effects, but we neglect this in our scaling analysis. The results shown in this section follow from balancing static forces in equation (2.13), although dynamics have an

effect since apparent contact angles at the edges of the pool, which may be finite in truly static situations, must be zero where a thin film is pulled out of the pool. These results will be important in explaining the thickness of the film which coats the sides and top of the cylinder, which will be analysed in § 3.2.

There are two subcases, according to the balance of parameters: in one case the first-order gravity term (IV) is larger than the leading-order surface tension term (III) and the dominant (static) balance is between the leading-order (II) and first-order (IV) gravitational terms; as explained below, this occurs when $\mathscr{B}^{-3/5} \ll A \ll 1$ and is the case which is more likely to be observed. In the other case, the balance is between leading-order gravitational effects (II) and surface tension (III), since the latter are greater than the first-order gravity effects. Then the balance of parameters is shown to be $A \ll \mathscr{B}^{-3/5} \ll 1$.

We first consider the dominant balance between leading-order and first-order gravity terms. The requirement that $A \gg \mathscr{B}^{-3/5}$ can be rewritten as $R \gg A^{-1/3}(\gamma/\rho g)^{1/2}$, where $(\gamma/\rho g)^{1/2}$ is the usual capillary length. Consequently the radius is large in comparison to the capillary length and a flat pool forms at the bottom of the cylinder.

In the pool typical values of θ are small, so we use the approximation $\sin\theta \approx \theta$. In equation (2.13), balancing leading-order (II) and first-order (IV) gravity terms gives $\lambda h_{\max}^3 \Delta\theta \approx A\lambda h_{\max}^4/\Delta\theta$. Since only a small amount of fluid is pulled out of the pool, the integral boundary condition can only be satisfied if $\int_{-\theta^*}^{\theta^*} h(\theta)\,\mathrm{d}\theta \approx \pi$. (The assumption that only a small amount of fluid is pulled out of the pool will be seen to hold in § 3.2, where we shall obtain an expression for the film thickness.) These two conditions yield the following functional form for $h(\theta)$ in the pool and scalings for the pool height and width:

$$h(\theta) = \frac{1}{A}\log\left(\frac{\cos\theta}{\cos\theta^*}\right), \qquad h_{\max} \approx \frac{1}{2A}\left(\frac{3\pi A}{2}\right)^{2/3}, \quad \Delta\theta \approx \left(\frac{3\pi A}{2}\right)^{1/3}, \quad (3.1)$$

where θ^* is a measure of the extent of the static pool, as is indicated in figure 3. Note that $\theta^* \approx \Delta\theta$ (since $\theta^* \approx 2\theta_1 \approx 4\pi - 2\theta_2$). These results for the flat pool in the gravity-dominated case could, of course, have been anticipated from a simple geometric argument, and are in agreement with the pool profile generated in the numerical simulation.

Tirumkudulu & Acrivos (2001) give a discussion of a solution for the pool region when $\mathscr{B}^{-3/5} \ll A$ which is in fact valid for $A < 1/2$, i.e. when the extent of the pool θ^* takes any value less than $\pi/2$. In their notation, these constraints correspond to $\mathscr{C} \gg F^{4/3}/\beta^2 = \alpha^2/F^{2/3}$ and $F < 1/2$. Tirumkudulu & Acrivos (2001) introduced a first-order gravity term into their flux equation which had the feature that the correct solution for $h(\theta)$ is obtained in the absence of flow in the limit of zero surface tension. A different first-order gravity term is included in equation (2.13) which is asymptotically valid for $A \ll 1$. The solution (3.1) is valid when $\theta^* \ll 1$ which, since $\theta^* \approx A^{1/3}$, is consistent with the condition for the flux equation to be valid, $A \ll 1$. The expression for the shape of the interface in the pool region (3.1) agrees at leading order with the small-angle limit ($\theta^* \ll 1$) of the solution in the pool derived by Tirumkudulu & Acrivos (2001).

A more detailed analysis shows that the pool solution (3.1) has a non-zero contact angle as $\theta \to \theta^*$, and therefore at the edges of the pool there is a static meniscus where gravity balances surface tension in order to satisfy the zero effective contact angle condition. Although the scaling can be derived by considering only linear curvature terms, the nonlinear curvature terms are important in obtaining the exact solution.

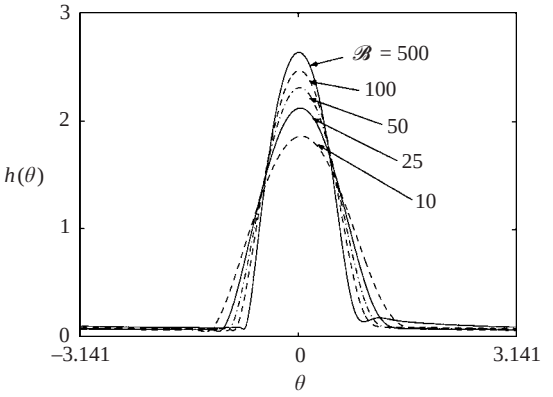

FIGURE 5. Plot of numerical solution to equation (2.13) with varying Bond number. In each case, $\lambda = 50$ and $A = 0.1$. (Note that the range is $-\pi \leqslant \theta \leqslant \pi$.)

The overall structure of the film profile in this case involves three regions: an outer pool region, an intermediate matching region and an inner film region, as described in more detail in § 3.2.

On the other hand, when $A \ll \mathscr{B}^{-3/5}$, the radius is small in comparison to the capillary length and the pool that forms has a surface-tension-induced non-zero curvature. As shown in figure 5, in this limit the shape of the pool varies according to the value of the Bond number; in particular, the pool is narrower and deeper for larger Bond numbers.

We assume that $|h'| \ll A^{-1}$ (to be verified later) so that for our analytic estimates the curvature in term (III) of equation (2.13) can be approximated linearly by $h + h''$, as discussed in § 2.2, and also that $|h'''| \gg |h'|$ as is usual in boundary-layer approximations. A quantitative calculation of the interface shape in the static pool can be made by balancing terms (II) and (III) in equation (2.13):

$$\mathscr{B} \sin\theta = h''' \quad \Rightarrow h(\theta) = \mathscr{B} \cos\theta + c_1\theta^2 + c_2\theta + c_3, \tag{3.2}$$

where c_1, c_2 and c_3 are constants to be determined. We assume that the pool is symmetric since the viscous forces are weak relative to the gravitational and surface tension forces (i.e. fluid motion is negligible in the pool) which leads to the boundary condition $h'(0) = 0$. The other boundary conditions are

$$h(\theta^*) = 0, \quad h'(\theta^*) = 0, \quad \int_{-\theta^*}^{\theta^*} h(\theta)\,\mathrm{d}\theta \approx \pi, \tag{3.3}$$

where $h'(\theta^*) = 0$ represents the zero contact angle condition. The interface height in the pool is given by

$$h(\theta) = \mathscr{B}\left(\cos\theta + \frac{\sin\theta^*}{2\theta^*}\theta^2 - \cos\theta^* - \frac{\theta^* \sin\theta^*}{2} \right), \tag{3.4}$$

where the integral condition of equation (3.3) is used to determine θ^*. Since $\mathscr{B} \gg 1$ and therefore $\theta^* \ll 1$, we can perform a small-angle expansion of the trigonometric terms in the expression for θ^* which leads to the prediction

$$\theta_1 - \theta_2 + 2\pi \approx \theta^* = \left(\frac{45\pi}{2} \right)^{1/5} \mathscr{B}^{-1/5}. \tag{3.5}$$

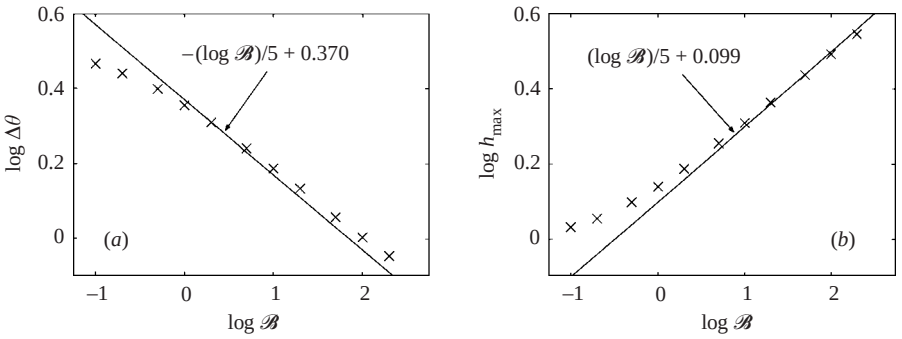

FIGURE 6. Scaling of (*a*) $\Delta\theta$ and (*b*) $h_{\max}$ for the pool in the bottom of the cylinder, as defined in § 3.1. The solid lines represent the scaling expected from (3.5) and (3.6) and the points are the data taken from the full numerical solution to (2.13). (Note that $\log(45\pi/2)^{1/5} = 0.370$, $\log[(45\pi/2)^{1/5}/24] = 0.099$.) $\lambda = 1000$ and $A = 0.01$ in all cases.

Similarly, we calculate the maximum interface height $h_{\max}$, approximated by $h(0)$, to be

$$h_{\max} \approx h(0) = \frac{1}{24}\left(\frac{45\pi}{2}\right)^{4/5} \mathscr{B}^{1/5}. \tag{3.6}$$

These results have been confirmed numerically. Figures 6(*a*) and 6(*b*) compare the results of (3.5) and (3.6), the solid lines, with data extracted from many numerical simulations. The scaling breaks down when the Bond number $\mathscr{B}$ becomes too small, as expected, which here is for $\mathscr{B} \lesssim 3$. Physically, at this point the width $\Delta\theta$ is no longer small and this affects not only the scaling of $\Delta\theta$ but also the scaling of the film thickness, which is discussed in detail below. We note that it has been possible to determine a pool solution with a zero contact angle using only the linearized curvature, as just justified, in the analytical arguments. The validity of using the linearized curvature in the analysis is confirmed by the good agreement between the theoretical prediction and the numerics, which include the full nonlinear curvature term.

The leading-order gravity and surface tension terms in (2.13) are both $O(\lambda\mathscr{B}^{2/5})$ and the first-order gravity term (IV), which we have neglected, is $O(A\lambda\mathscr{B})$, and so this analysis rests on the assumption that $A \ll \mathscr{B}^{-3/5} \ll 1$. Also, since $|h'| \approx \mathscr{B}^{2/5}$ and $\mathscr{B} \gg 1$, gradients in this non-dimensionalization are large, and therefore it is necessary to check that the linear approximation of the curvature is valid. With (2.9) this simplification requires $O(A|h'|) \ll 1$, and we see that the above scaling results require $A \ll \mathscr{B}^{-2/5}$. Since $\mathscr{B}$ is large, the stronger of these two conditions is $A \ll \mathscr{B}^{-3/5} \ll 1$. In the next section we shall use matched asymptotics to determine the complete thickness profile, where the pool is the outer region and the film is the inner region.

3.2. *The thin film connected to the pool*

We now consider the thin film that emanates from and leads back into the pool. The thin film has small curvature variations and therefore surface tension has little effect on the flow in the film itself, though nevertheless may set the film thickness through its action in the neighbourhood where the film is pulled from the pool.

We define the film thickness $h_{\text{film}} = h(\pi)$, as shown in figure 4. The variations in the film thickness due to gravity and surface tension effects are small in comparison to

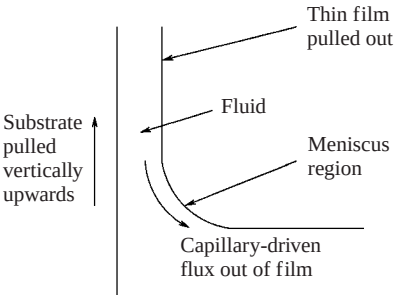

FIGURE 7. The Landau–Levich–Derjaguin problem: pull-out of a thin film when a substrate is withdrawn vertically from a fluid bath.

the thickness of the film and so h_{film} can be taken to describe the order of magnitude of the approximately constant film thickness. In the limit that surface tension effects can be neglected, a balance of the viscous and leading-order gravitational terms in equation (2.13) for $\lambda \gg 1$ leads to the prediction

$$h_{\text{film}} \approx \lambda^{-1/2}. \tag{3.7}$$

Furthermore in the complete absence of surface tension and first-order gravity terms, as mentioned earlier, there is no steady solution for $\lambda \gtrsim 5$. However, we shall show that for $\lambda \gg 5$ when surface tension effects are important, a scaling prediction as in (3.7) is incorrect as the film thickness is set at a point leaving the pool where the curvature variations are large. In other words, a capillary-pressure-driven flux occurs in the thin film that counters the flux produced by viscous stresses (see figure 7). To demonstrate the influence of non-zero surface tension we show below numerical results of steady solutions with a scaling for h_{film} dependent on λ and $\mathscr{B}$, which is different from (3.7).

The mechanism producing these new steady thin-film profiles is identical to that in the Landau–Levich–Derjaguin pull-out problem (Derjaguin 1943; Landau & Levich 1942; Wilson 1981), which describes the thickness of the film deposited on a flat plate or cylindrical fibre when pulled vertically out of a fluid reservoir at constant velocity (see figure 7), and which appears in numerous other withdrawal problems (Bretherton 1961; Quéré 1999; Ratulowski & Chang 1989; Wilson & Jones 1983), though it has not previously been recognized in the rimming flow problem. The average film thickness is determined by asymptotically matching the curvature of the interface where the film is pulled out of the pool and in the meniscus at the edge of the pool. This structure is illustrated in figure 8.

As we have described in § 3.1, there are two possible pool shapes depending on the balance of parameters. These give rise to two different film thicknesses. We now describe the detailed analysis of the thin-film section treating both cases together, and then separately describe the curvature matching to the outer pool region. In the inner film region, equation (2.13) is written in terms of the rescaled variables

$$H(\Theta) = \frac{h(\theta)}{q_i}, \quad \Theta = \left(\frac{3\mathscr{B}}{q_i^3\lambda}\right)^{1/3}(\theta - \theta^*), \tag{3.8}$$

where θ^* is the angle at which the film is pulled out of the pool, indicated in figure 3. We use a subscript on the flux q_i since the value of the flux in the case $A \gg \mathscr{B}^{-3/5}$,

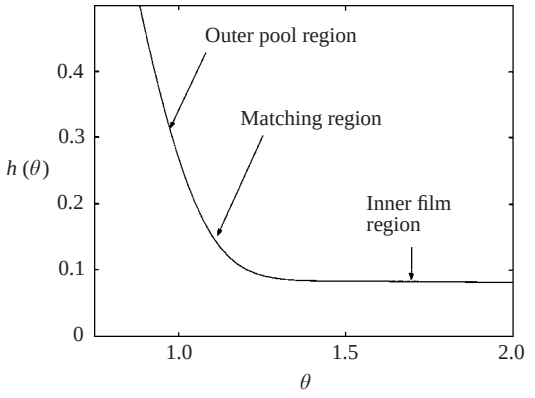

FIGURE 8. The structure of the solution with the outer pool, matching and inner film regions.

q_{I}, will differ from that in the case $A \ll \mathscr{B}^{-3/5}$, q_{II}. $H(\Theta)$ satisfies

$$1 = H - \frac{\lambda q_i^2 H^3}{3} \sin\left[\left(\frac{\lambda q_i^3}{3\mathscr{B}}\right)^{1/3} \Theta + \theta^*\right] + H^3\left[\left(\frac{\lambda q_i^3}{3\mathscr{B}}\right)^{2/3} \frac{\mathrm{d}H}{\mathrm{d}\Theta} + \frac{\mathrm{d}^3 H}{\mathrm{d}\Theta^3}\right] \quad (3.9a)$$

$$H(\Theta \to \infty) \to 1. \quad (3.9b)$$

It can be verified *a posteriori* that the higher-order terms of (2.13) are negligible in the film region, as assumed. In (3.10), we retain the terms that are of leading order in the thin film, namely the viscous terms (1 and H), and highest derivative term arising from surface tension, $H^3 H_{\Theta\Theta\Theta}/3$. (The restriction, in terms of an effective capillary number, which arises from the assumption that the leading-order gravitational terms are negligible is derived later in this section.) Equation (3.9) reduces to

$$1 = H + H^3 \frac{\mathrm{d}^3 H}{\mathrm{d}\Theta^3}, \quad H(\Theta \to \infty) \to 1, \quad (3.10)$$

which is, in fact, the Landau–Levich–Derjaguin problem (Derjaguin 1943; Landau & Levich 1942). Numerically integrating this equation backwards out of the thin film towards the pool, starting from a numerical approximation to the boundary condition at $\Theta \to \infty$, we obtain $H''(0) = 0.643$. Then the curvature in the original dimensionless variables is

$$h''(\theta^*) = \frac{3^{2/3} H''(0) \mathscr{B}^{2/3}}{q_i \lambda^{2/3}} \quad (3.11)$$

and this must be matched to the (known) curvature of the meniscus at the edge of the pool to obtain the flux q_i.

We derive the film thickness by matching to the curvature of the meniscus separately for the two cases $A \gg \mathscr{B}^{-3/5}$ and $A \ll \mathscr{B}^{-3/5}$. First, we consider the limit where the pool balance is between leading-order (II) and first-order (IV) gravity forces, $A \gg \mathscr{B}^{-3/5}$, as discussed in § 3.1. This feature of the problem is an extension of the Landau–Levich–Derjaguin problem in which a plate is withdrawn vertically from a fluid bath, and is closely related to a study by Wilson (1981), who investigated the film coating both the outside of a rotating cylinder, partially immersed in a fluid bath, and an inclined flat plate withdrawn from a fluid bath. The curvature of the usual static meniscus derived from the full nonlinear Young–Laplace equation using

our non-dimensionalization is

$$\frac{h_{\rm sm}}{\ell_{\rm sm}^2} \approx \sqrt{\frac{2\mathscr{B}(1-\cos\theta^*)}{A}}, \tag{3.12}$$

where $h_{\rm sm}$ represents the order of magnitude of the film height in the static meniscus and $\ell_{\rm sm}$ represents that of the length scale over which the static meniscus exists. This result can be obtained by integrating the gravity (II), surface tension (III) and first-order gravity (IV) terms of the flux equation (2.13). The dependence on filling fraction A and Bond number $\mathscr{B}$ can be rewritten in the more familiar dimensional form as

$$\frac{h_{\rm sm}}{\ell_{\rm sm}^2} \approx \sqrt{\frac{2\rho g(1-\cos\theta^*)}{\gamma}}. \tag{3.13}$$

Equating equations (3.11) and (3.12) yields the curvature matching condition typical of these problems:

$$h''(\theta^*) = \frac{3^{2/3}H''(0)\mathscr{B}^{2/3}}{q_i\lambda^{2/3}} = \sqrt{\frac{2\mathscr{B}(1-\cos\theta^*)}{A}} \tag{3.14a}$$

$$\Rightarrow q_{\rm I} = h_{\rm film_I} = \frac{0.946}{(1-\cos\theta^*)^{1/2}}\frac{A^{1/2}\mathscr{B}^{1/6}}{\lambda^{2/3}} \approx 0.798\frac{A^{1/6}\mathscr{B}^{1/6}}{\lambda^{2/3}}. \tag{3.14b}$$

The expression for the angle of withdrawal of the film from the pool θ^* is taken from (3.1), $\theta^* \approx (3\pi A/2)^{1/3}$. In deriving this result we have assumed that we can approximate the gravitational force $\lambda h(\theta)^3\sin\theta/3$ by $\lambda h(\theta)^3\sin\theta^*/3$ in the meniscus region, which Wilson (1981) shows corresponds to the requirement that $R \gg \sqrt{\gamma/\rho g}$ or equivalently $\mathscr{B} \gg A^{-1} \gg 1$. Finally, neglecting the leading-order gravity term in the analysis of (3.9) requires that the condition $\lambda q_i^2\theta^* \ll 1$ be satisfied (using the small-angle approximation $\sin\theta^* \approx \theta^*$), which in this limit results in the condition $A^2\mathscr{B}/\lambda \ll 1$. $A^2\mathscr{B}/\lambda$ is an effective capillary number. More detailed analysis shows that the expression for film thickness (3.14*b*) is the leading-order term in an expansion in terms of the parameter $A^2\mathscr{B}/\lambda$, and the result (3.14*b*) is asymptotically valid in the limit $A^2\mathscr{B}/\lambda \to 0$. All restrictions on the analysis are summarized in table 2. (We note that (3.14*b*) simplifies to the Landau–Levich–Derjaguin result when $\theta^* = \pi/2$, and that Wilson calculated the next term, of order $A^{3/2}\mathscr{B}^{1/2}\sin\theta^*/\lambda(1-\cos\theta^*)^{3/2}$.)

We verify the theoretical prediction of the film thickness dependence on λ and Bond number $\mathscr{B}$ by comparing with the results of many numerical simulations. By plotting the flux $q_{\rm I}$ as a function of λ and $\mathscr{B}$ we have verified numerically that the scaling with respect to the gravitational parameter λ is correct. Typical results are shown in figure 9(*a*). Since the dependence on Bond number is weak, we have also plotted $q_{\rm I}\lambda^{2/3}$ as a function of $\mathscr{B}$ alone to verify the scaling with respect to the Bond number $\mathscr{B}$. These results are shown in figure 9(*b*), where results are given over more than one order of magnitude for $\mathscr{B} \gg 1$. The theoretical value of the numerical prefactor is in very good agreement with our numerical simulations.

Secondly, when $A \ll \mathscr{B}^{-3/5} \ll 1$ and the pool balance is between leading-order gravitational forces and surface tension forces, it is necessary to use a different curvature matching condition since the curvature of the pool solution in the outer region differs from that of the usual static meniscus. The curvature in the pool region which enters the matching condition is now given by differentiating equation (3.4)

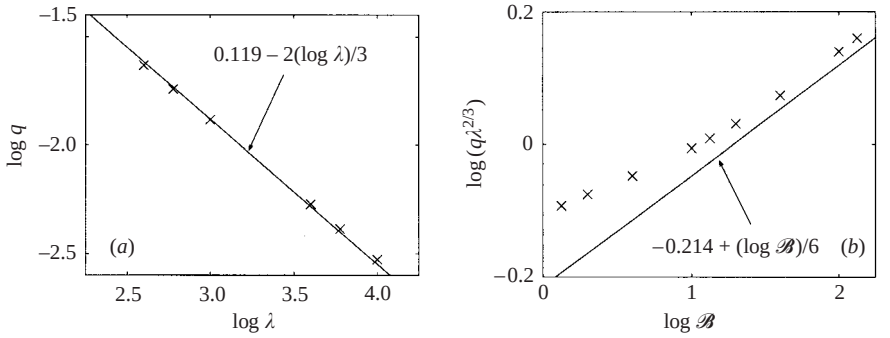

FIGURE 9. Scaling of flux q_{I} when $A^2\mathscr{B}/\lambda \ll 1$, $\mathscr{B}^{-3/5} \ll A \ll 1$. The points represent numerical results based on (2.13) and the lines are the analytical predictions following from (3.14*b*). (*a*) Variation with λ. $\mathscr{B} = 100$ and $A = 0.2$ for all data. (Note that $\log(0.798A^{1/6}\mathscr{B}^{1/6}) = 0.119$.) (*b*) Variation with Bond number. $\lambda = 10000$ and $A = 0.2$ for all data. (Note that $\log(0.798A^{1/6}) = -0.214$.)

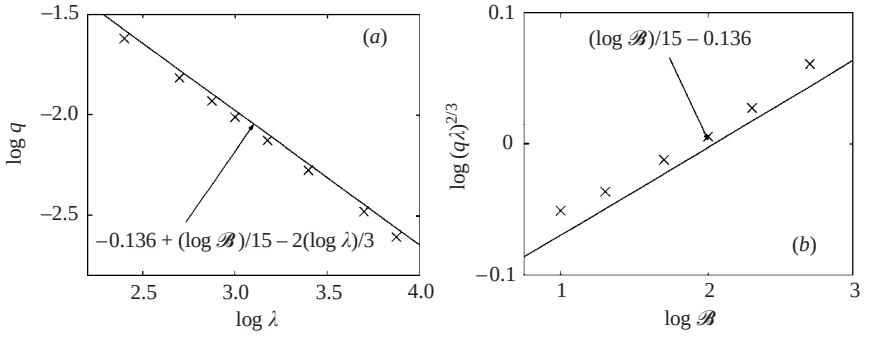

FIGURE 10. Scaling of flux q_{II} when $\mathscr{B}^{-3/5} \gg A$. The points represent numerical results and the lines the analytical predictions following from (3.15*b*). (Note that $\log 0.731 = -0.136$.) (*a*) Variation with λ. $\mathscr{B} = 50$ and $A = 0.01$ for all data. (*b*) Variation with Bond number. $\lambda = 1000$ and $A = 0.01$ for all data.

and expanding about $\theta = \theta^*$, leading to the matching condition

$$\frac{3^{2/3}H''(0)\mathscr{B}^{2/3}}{q_{\mathrm{II}}\lambda^{2/3}} = \frac{1}{3}\left(\frac{45\pi}{2}\right)^{2/5}\mathscr{B}^{3/5} \tag{3.15a}$$

$$\Rightarrow q_{\mathrm{II}} = h_{\mathrm{film_{II}}} = 0.731\frac{\mathscr{B}^{1/15}}{\lambda^{2/3}}. \tag{3.15b}$$

As in the derivation of (3.14), the analysis to obtain (3.15) rests on the assumption that $\mathscr{B} \gg A^{-1} \gg 1$. In this case the condition $\lambda q_i^2\theta^* \ll 1$, which arises from neglecting the gravity term in the analysis of (3.9), corresponds to the requirement that $\mathscr{B}^{-1/5}\lambda^{-1} \ll 1$. (In table 2 we indicate how the parameter $\mathscr{B}^{-1/5}\lambda^{-1}$ can be rewritten in terms of the effective capillary number $A^2\mathscr{B}/\lambda$, and summarize all the conditions necessary for the analysis to hold.)

Numerical solutions based on (2.13) and the full curvature are shown in figure 10 and are compared with the asymptotic dependence predicted by (3.15*b*). The agreement between the numerical and asymptotic results for dependence on λ and $\mathscr{B}$ is very good.

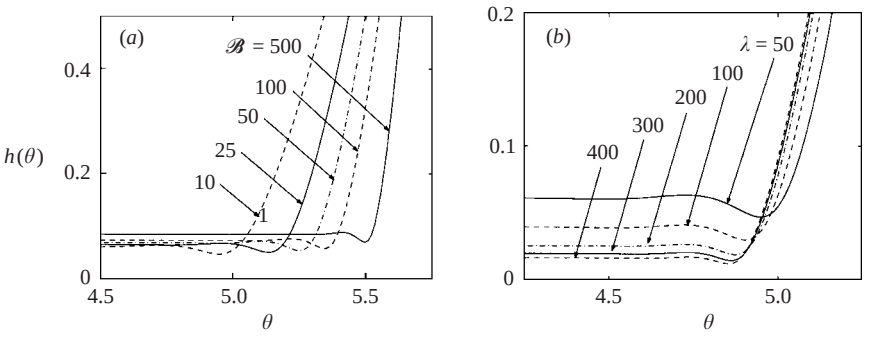

FIGURE 11. Numerical results showing the occurrence of dimples (*a*) when $\lambda = 50,\ A = 0.1$, (*b*) when $\mathscr{B} = 10,\ A = 0.1$.

The above results have demonstrated that at low effective capillary numbers the singular effect of surface tension is significant. By including surface tension we have found numerically steady solutions that agree with predicted scaling arguments. In terms of the physical variables, the dimensional film thicknesses in the two cases discussed above are

$$h_{\mathrm{film_I}} = 0.798\frac{(\mu\Omega R)^{2/3}}{A^{1/3}(\rho g)^{1/2}\gamma^{1/6}}, \qquad h_{\mathrm{film_{II}}} = 0.731\frac{(\mu\Omega)^{2/3}R^{7/15}}{A^{2/5}(\rho g)^{3/5}\gamma^{1/15}}, \tag{3.16}$$

valid in the limits $\mathscr{B}^{-3/5} \ll A \ll 1$ and $A \ll \mathscr{B}^{-3/5} \ll 1$ respectively. The restrictions on the analysis of both the pool and film region for the two solutions in the limit $\lambda \gtrsim 5$ are summarized in table 2.

3.3. *The dimple*

Figure 11(*a*, *b*) shows the region of the interface where the thin film re-enters the pool and a dimple occurs. Such dimples are a universal feature of free surfaces in regions where surface tension must smooth the sudden transition from a thin film to a region with large curvature variations. Similar dimples are seen in other problems such as when a falling film enters a pool (Wilson & Jones 1983), the translation of large bubbles in fluid-filled capillary tubes described by Bretherton (Bretherton 1961, see also Ratulowski & Chang 1989), in the Marangoni-driven motion of thin films (Bertozzi, Munch & Shearer 1999) and in problems in which thin films line cylindrical tubes (Jensen 1997).

In general, the region where a film enters a pool has a complex structure in which ripples occur, each of which has a quantitatively different height scale and occurs over a qualitatively different length scale, as shown by Wilson & Jones (1983). (Theoretically, the ripples extending upstream into the thin film are infinite in number but in reality they are damped so quickly that it is rare that more than one oscillation is observed.) We briefly review the mathematical ideas of Wilson & Jones (1983) to show how the structure of the equations leads to oscillatory behaviour in the film on the side where it enters the pool but not on the side where the film is withdrawn from the pool (Bretherton 1961; Wilson & Jones 1983). We consider the solution in the particular instance that $A \gg \mathscr{B}^{-3/5}$.

The asymptotic analysis in the vicinity of where the film re-enters the pool is exactly analogous to the analysis of the region where the film is pulled out, described in § 3.2. Again, there are three regions: the inner film region, and intermediate matching region and the outer pool region, as illustrated in figure 12. To analyse the initial

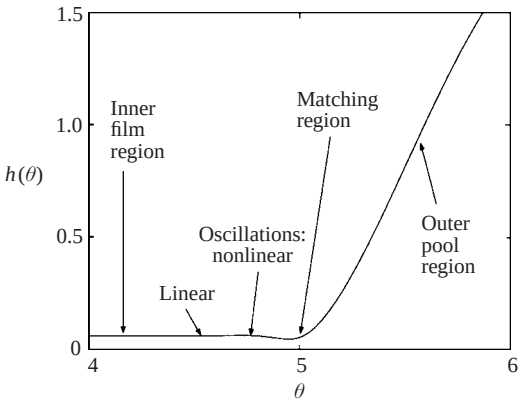

FIGURE 12. The three different regions in the vicinity of the dimple, also indicating the regions where linear and nonlinear oscillations occur.

small deviations from the film of uniform thickness we rescale $h(\theta)$ as in (3.8), and rescale θ analogously

$$\phi = (\theta - 2\pi + \theta^*)\left(\frac{3\mathscr{B}}{q_1^3\lambda}\right)^{1/3}. \tag{3.17}$$

We obtain the same equation but a different boundary condition compared to (3.10):

$$H_{\phi\phi\phi} = \frac{1}{H^3} - \frac{1}{H^2}, \quad H(\phi \to -\infty) \to 1. \tag{3.18}$$

The boundary condition differs simply because rather than looking at the region where the thin film is pulled from the pool, we are focusing here on where it re-enters the pool. As $\phi \to -\infty$ the solution H exhibits a decaying harmonic oscillation about the constant value 1. This follows from substituting $H(\phi) = 1 + \epsilon(\phi)$ into (3.18) where $\epsilon \ll 1$ and linearizing in ϵ to obtain $\epsilon_{\phi\phi\phi} = -\epsilon$, which has roots $\epsilon = \mathrm{e}^{\eta_k \phi}$, $k = 1, 2, 3$ where $\eta_1 = -1$, $\eta_{2,3} = (1 \pm \mathrm{i}\sqrt{3})/2$. The solution must be bounded as $\phi \to -\infty$ in order to match to the uniform film and therefore the root arising from η_1 can be eliminated and a second root can be eliminated as well by a suitable choice of origin. Since the chosen root has an imaginary part, the film exhibits decaying sinusoidal oscillations as $\phi \to -\infty$. Conversely, at the point where the film is pulled out from the pool, the solution must be bounded as $\phi \to \infty$ and the appropriate root is -1, which implies that the interface height decays monotonically to the constant film thickness. These features are all reproduced in our numerical simulations.

As ϕ increases, the size of the oscillations increases and the linear approximation used above breaks down. Nonlinear oscillations develop and can be analysed using the methods of Wilson & Jones (1983). As in their problem, the film depth in the final trough (visible as a dimple in our numerical results) is set by matching the curvature to that of the static meniscus, which in the case $A \gg \mathscr{B}^{-3/5}$ involves consideration of both the gravitational term and also the full nonlinear curvature in the surface tension term. The details are different, however, and the analogous analysis leads to the prediction that in this case the scaling of the interface height with λ and Bond number $\mathscr{B}$ at the dimple h_{dimple}, is identical to that of the film, h_{film}. In figure 13 numerical results are shown for the dimple height, defined as the smallest thickness in the region of re-entry, to verify the scaling with respect to λ.

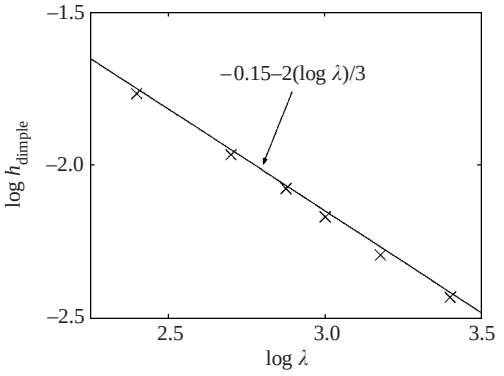

FIGURE 13. Numerical results showing that $h_{\text{dimple}} \approx O(\lambda^{-2/3})$ with $\mathscr{B} = 5,\ A = 0.3$.

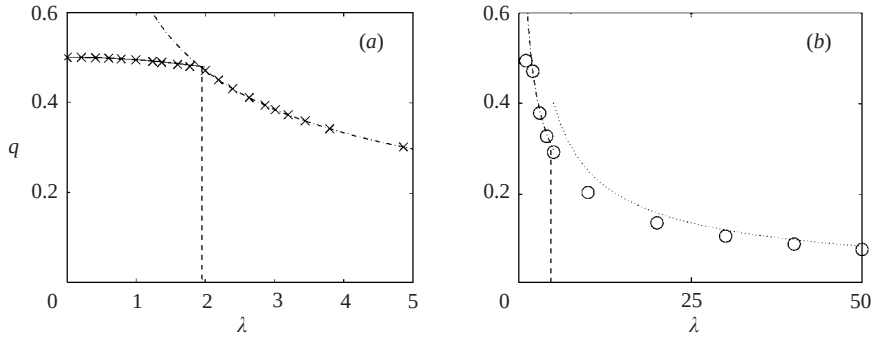

FIGURE 14. (*a*) Plot of flux q as a function of λ in the theoretical limit of zero surface tension neglecting terms $O(A,\ A\lambda)$. Crosses represent numerical results and the dot-dash curve represents the theoretical prediction, $q = 2/3\sqrt{\lambda}$, for $2.00 \leqslant \lambda \leqslant 4.86$. The solid curve represents the theoretical prediction for $\lambda \leqslant 2$, described in Appendix D (D 6*b*). The vertical dashed line marks the transition to discontinuous shock solutions. (*b*) Plot of flux q as a function of λ when surface tension and first-order gravity effects are included. Circles represent the results for fixed finite Bond number $\mathscr{B} = 100,\ A = 0.1$. The dot-dash curve represents the theoretical prediction when surface tension and first-order gravity effects are neglected, $q = 2/3\sqrt{\lambda}$ for $2.00 \leqslant \lambda \leqslant 4.86$ (as in (*a*)), which remains a good approximation in the non-zero surface tension case. The dotted curve indicates the theoretical prediction (3.14*b*). The vertical dashed line indicates the largest value of λ for which the zero surface tension solution exists when first-order gravity terms are also neglected.

The reason for this simple result is that the film thickness has been set to satisfy a balance between viscous and surface tension forces and to match to the curvature of the pool solution when it is drawn out. The film still satisfies these conditions when it re-enters the pool since the effects of gravity in the thin film are too small to alter the film thickness at leading order.

3.4. *Flux*

The relationship between the flux q and the gravitational parameter λ with surface tension and first-order gravity effects neglected was established analytically by Moffatt (1977) and verified numerically by Benjamin *et al.* (1993), and is shown in figure 14(*a*).

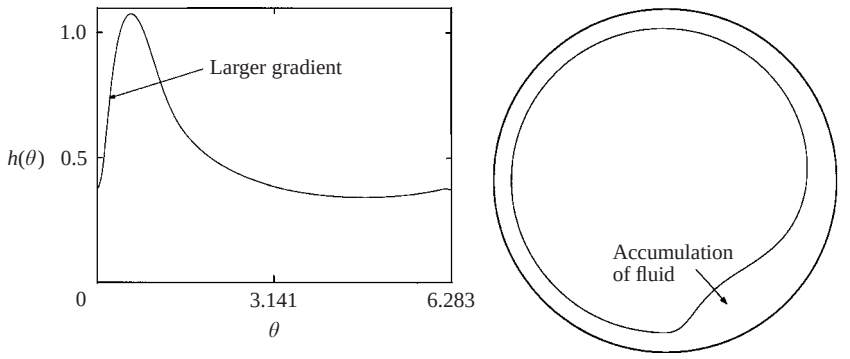

FIGURE 15. Plot of numerical solution to equation (2.13) with $\lambda = 3$, $\mathscr{B} = 1000$, $A = 0.3$, showing the larger interfacial gradient at the edge of the region where fluid accumulates in the quadrant $0 \leqslant \theta \leqslant \pi/2$.

This graph shows that when surface tension and first-order gravity are neglected, the flux takes a value close to 1/2 when $\lambda \lesssim 2$, and when $2 \lesssim \lambda \lesssim 5$, the flux takes the exact value $q = 2/3\sqrt{\lambda}$. (The small reduction in flux as λ increases from $0 \rightarrow 2$ is discussed in Appendix D and the results for $2 \lesssim \lambda \lesssim 5$ will be discussed in § 4.)

If $\lambda \gtrsim 5$, no steady solutions are predicted in the zero surface tension case when first-order gravity terms are also neglected (Moffatt 1977). Figure 14(*b*) shows the flux values of the steady solutions as a function of λ that are obtained numerically when surface tension and first-order gravity effects are included at small effective capillary numbers $A^2\mathscr{B}/\lambda \ll 1$. Our theoretical predictions for the value of the flux, given by equation (3.14*b*), are also plotted for comparison. The numerical results show that the theory incorporating surface tension provides a good prediction for $\lambda \gtrsim 25$. (The relationship between the flux q and λ in this limit has already been shown to be $q \approx A^{1/6}\mathscr{B}^{1/6}/\lambda^{2/3}$ when $\mathscr{B}^{-3/5} \ll A \ll 1$ in figure 9.) In the limit that $\lambda \gtrsim 5$, $\mathscr{B}^{-3/5} \ll A \ll 1$ and the effective capillary number $A^2\mathscr{B}/\lambda \gg 1$, the solution described by Tirumkudulu & Acrivos (2001) (in which surface tension is negligible) is valid and the corresponding flux is $q = 2/3\sqrt{\lambda} + O(A)$ (Tirumkudulu & Acrivos 2001).

4. Numerical and scaling results: $2 \lesssim \lambda \lesssim 5$

When $2 \lesssim \lambda \lesssim 5$, the scaling results derived in the previous section in the limit $\lambda \gg 5$ are no longer accurate. Rather than having a pool structure with the fluid sitting in the bottom of the cylinder, in the limit $2 \lesssim \lambda \lesssim 5$ the viscous and gravitational forces are of the same order of magnitude and some fluid is pulled up the sides and over the top of the cylinder but some accumulates on the rising side of the cylinder. A numerical solution of equation (2.13) for $h(\theta)$ in the non-zero surface tension case is shown in figure 15, which illustrates the region where fluid accumulates. At the front of this region the gradient of the interface is larger, and the solution exhibits a strong asymmetry about $\theta = 0$.

We briefly review in § 4.1 the established results for the case $2.00 \leqslant \lambda \leqslant 4.86$, which mainly concern the zero surface tension limit in which first-order gravity effects are also neglected, and in § 4.2 we present results describing the effect of surface tension on the film thickness for this range of λ.

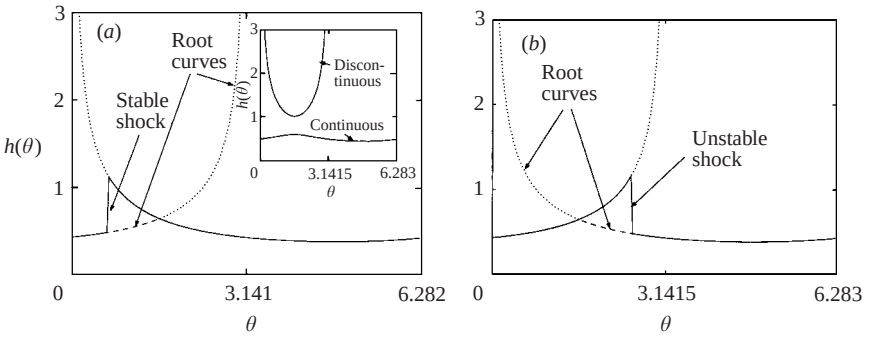

FIGURE 16. Plot of numerical solution to the flux equation in the zero surface tension case when first-order gravity effects are also neglected, showing (*a*) a stable and (*b*) an unstable shock when $\lambda = 2.40$, $q = 2/3\sqrt{\lambda} = 0.43$. The inset shows a plot of the numerical solution to the flux equation when surface tension and first-order gravity are neglected with $\lambda = 1.52$, $q = 0.6$.

4.1. $2.00 \leqslant \lambda \leqslant 4.86$ *in the limit that surface tension and first-order gravity are neglected*

The flux equation (2.13) has been widely studied in the limit that surface tension and first-order gravity effects are neglected (Benjamin *et al.* 1993; Johnson 1988; Moffatt 1977; O'Brien & Gath 1988; Ruschak & Scriven 1976; Tirumkudulu & Acrivos 2001; Wilson & Williams 1997) in which case (2.13) reduces to a cubic algebraic equation and the solutions are discontinuous. Some representative solutions of this equation are shown in figure 16. Previous studies show that of the three roots of the cubic equation, one is negative and therefore unphysical, one is discontinuous and the other is continuous. Figure 16 shows the continuous (inset) and discontinuous solution curves.

If $2.00 \leqslant \lambda \leqslant 4.86$, $q = 2/3\sqrt{\lambda}$, the two positive roots meet at $\theta = \pi/2$ (Benjamin *et al.* 1993). Then, as illustrated in figure 16, the solution may 'jump' from the positive continuous root curve up to the positive discontinuous root curve in the first quadrant and transfer back to the positive continuous root curve at $\theta = \pi/2$ (O'Brien & Gath 1988). The position of the jump is chosen such that the integral boundary condition, approximated according to the assumption $A \ll 1$,

$$\int_0^{2\pi} h(\theta)\,\mathrm{d}\theta \approx \pi \tag{4.1}$$

is satisfied. Although 'jumps' satisfying this condition can be chosen in an infinite number of ways, the only choice which results in a stable solution is when the solution curve jumps up from the positive continuous curve to the positive discontinuous curve in the first quadrant and then transfers back to the positive continuous curve at $\theta = \pi/2$, as shown in figure 16 (Benjamin *et al.* 1993). When $\lambda < 2.00$ the integral condition is satisfied by the positive continuous root and no jump occurs; however, as λ increases from 2.00 to 4.86 a shock develops at $\theta = \pi/2$ and moves towards $\theta = 0$.

In practice, when surface tension and first-order gravity effects are neglected, it is easier to calculate the critical values $\lambda = 2.00$ and $\lambda = 4.86$ by rescaling as in Benjamin *et al.* (1993), taking the (rescaled) flux $q = 2/3$ and calculating the filling fraction for two solutions: first, for the positive continuous root curve with no jump to the positive discontinuous root curve, and secondly, for a solution with a discontinuity at

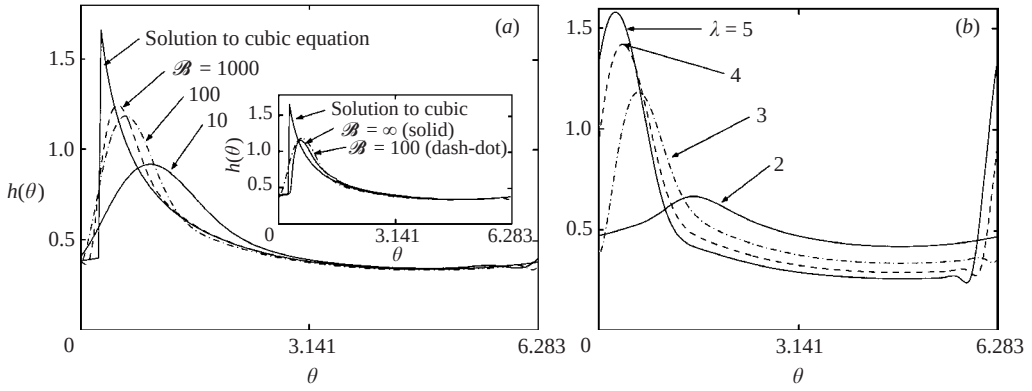

FIGURE 17. (*a*) Plot of numerical solution to the full equations (2.13) with $\lambda = 3$, $A = 0.1$ and $\mathscr{B} = 10,\ 100,\ 1000$. Also shown is the solution to the truncated flux equation with both surface tension and first-order gravity terms neglected. The solutions show smaller-amplitude, broader regions of shape variation occurring for larger values of surface tension. The inset shows the solution to the equation with infinite Bond number but including the first-order gravity term generated using the numerical method described by Tirumkudulu & Acrivos (2001). Also shown are the solution to the cubic equation in which both surface tension and first-order gravity effects are neglected, and the solution for $\mathscr{B} = 100$ when both surface tension and first-order gravity effects are neglected. (*b*) Solution to (2.13) with λ varying, Bond number $\mathscr{B} = 100$ and filling fraction $A = 0.1$.

$\theta = 0$. (Note that the positive discontinuous root curve has an integrable singularity at $\theta = 0$.) The critical values are then given by the square of the filling fraction. Using our dimensionalization, the equivalent calculation would be to find the flux q such that the solution is a positive continuous curve, and to find the flux q such that the solution has a discontinuity at $\theta = 0$. Then the critical values of the gravitational parameter could be determined via the relation $q = 2/3\sqrt{\lambda}$.

4.2. $2 \lesssim \lambda \lesssim 5$: *surface tension effects*

As mentioned above, in the zero surface tension limit in which first-order gravity effects are also neglected, the solution has a discontinuity at leading order and the lubrication approximation has broken down. It is necessary to consider first-order gravity or surface tension effects in a region close to where the jump occurs in order to obtain a continuous, physically realistic solution. Johnson (1988) and Tirumkudulu & Acrivos (2001) examined numerically the effect of smoothing by the first-order gravity term in the limit that surface tension is negligible and Benjamin *et al.* (1993) solved for $h(\theta)$ numerically, including the first-order gravitational term in both the zero and non-zero surface tension cases. Wilson, Hunt & Duffy (2002) analytically calculated the smoothing effect of first-order gravity in the particular case $\lambda = 2$, where $h(\theta)$ is continuous everywhere but $h'(\pi/2)$ is discontinuous.

We now extend the work of Benjamin *et al.* (1993) to include surface tension and first-order gravity terms and focus on the effect of different values of surface tension. It was verified numerically that the nonlinear curvature may be approximated by the linear curvature terms in this limit. Figure 17 provides numerical solutions that indicate both qualitative and quantitative features of the solution, and shows that as surface tension increases ($\mathscr{B}$ decreases), the region of significant shape variation (i.e. where gradients of $h(\theta)$ are larger) moves in the direction of increasing θ. These results are an extension of the observation made by Benjamin *et al.* (1993) that when

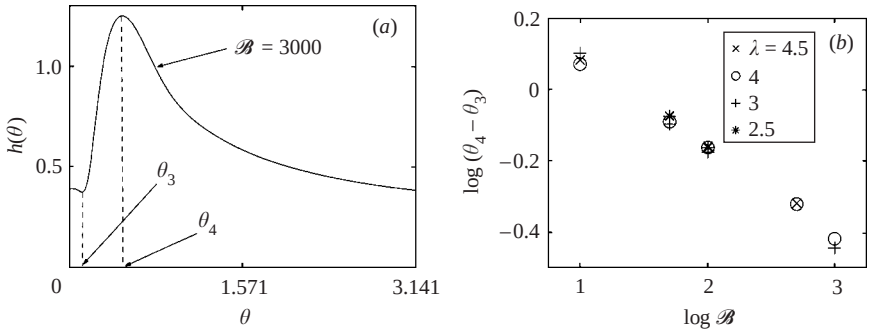

FIGURE 18. (*a*) Schematic showing definitions of θ_3 and θ_4. (*b*) Numerical data for $\theta_4 - \theta_3$ as a function of the Bond number $\mathscr{B}$. The scaling appears to be weakly dependent on λ. $A = 0.1$ in all cases.

surface tension is non-zero the region of shape variation occurs at a larger value of θ than (in the theoretical limit) when both surface tension and first-order gravity effects are neglected. Also, as surface tension increases, the difference in interface height just after and just before the region of shape variation decreases. The inset shows the numerical solution for $\mathscr{B} = 100$ and the solution obtained numerically with surface tension neglected but including the first-order gravity term (Tirumkudulu & Acrivos 2001), for which the solutions in the region of shape variation only differ by small amounts quantitatively.

We next consider the quantitative variations in the shape as the Bond number $\mathscr{B}$ is varied. Defining θ_3 to be the value of θ at which the local minimum occurs just before the region of shape variation and θ_4 to be that at which the local maximum occurs just after the region of shape variation, as indicated in figure 18(*a*), we can identify the following numerical scalings: $\theta_4 - \theta_3 \propto \mathscr{B}^{-\alpha(\lambda)}$ where $\alpha(2.5) = 0.2912$, $\alpha(3) = 0.2712$, $\alpha(4) = 0.2397$, $\alpha(4.5) = 0.2377$. The function $\alpha(\lambda)$ has been determined by a best-fit to the data shown in figure 18(*b*) and appears to be weakly dependent on λ.

It has not been possible to justify this numerical scalings via formal matched asymptotic expansions; however, some basic ideas can at least aid in qualitative and a semi-quantitative understanding. The simplest approach to determine how $\theta_4 - \theta_3$ scales with Bond number is to assume that in the vicinity of the region of shape variation, the viscous, gravity and surface tension terms are all of a similar magnitude (O'Brien & Gath 1988). When $\sin\theta \approx 1$, taking the outer solution to be $h \approx \sin\theta^{-1/2} \approx 1$ and balancing the viscous, gravitational and surface tension terms, we predict $\theta_4 - \theta_3 \propto \mathscr{B}^{-1/3}$. On the other hand if $\theta \ll 1$ then $\sin\theta \approx \theta$ and using an outer solution $h \approx \theta^{-1/2}$ (Benjamin *et al.* 1993; O'Brien & Gath 1988) leads to the prediction $\theta_4 - \theta_3 \propto \mathscr{B}^{-2/9}$. It is interesting to note that the exponents calculated numerically lie between these two theoretical values.

5. Discussion and concluding remarks

We have examined three different regimes of thin-film flow inside a horizontal rotating cylinder, covering a broad range of parameter space. Surface tension is important in a number of ways, as indicated in table 3. In particular, inclusion of surface tension sets the thickness of the thin film which coats the sides and top of the cylinder at small effective capillary numbers when $\lambda \gtrsim 5$. Also, non-zero surface

	Surface tension and first-order gravity neglected	Surface tension and first-order gravity included		
		$A^2\mathscr{B}/\lambda \gg 1$ $\mathscr{B}^{-3/5} \ll A \ll 1$	$A^2\mathscr{B}/\lambda \ll 1$ $\mathscr{B}^{-3/5} \ll A \ll 1$	$A^2\mathscr{B}/\lambda \ll A^2\mathscr{B}^{6/5} \ll 1$ $A \ll \mathscr{B}^{-3/5} \ll 1$
$5 \lesssim \lambda$	No steady solution	Surface tension unimportant	Surface tension important	
$2 \lesssim \lambda \lesssim 5$	Discontinuous	Region of shape variation Larger gradients reduced by first-order gravity or surface tension		
$\lambda \lesssim 2$	Small gravitational perturbation to uniform film; surface tension is unimportant			

TABLE 3. Summary of results in the zero and non-zero surface tension cases, divided according to the value of the gravitational parameter λ.

tension results in the occurrence of a dimple where the film re-enters the pool. When gravitational and viscous forces are of the same order of magnitude, discontinuities occur in the solutions to the equation with surface tension and first-order gravity neglected, and the solution may be made continuous by surface tension or by the first-order gravity term. Finally, when the ratio of gravitational to viscous forces is small, surface tension has little effect on the interface shape. Inclusion of the effects of surface tension has enabled us to obtain scaling relationships, in the spirit of the classical Landau–Levich–Derjaguin analysis, covering a broader range of parameter space than has previously been possible, as indicated in table 3.

The lubrication analysis used here is based on the assumption $A \ll 1$ since the interface height is non-dimensionalized by the factor AR. Now on the other hand, when $\lambda \gtrsim 5$, $\mathscr{B}^{-3/5} \ll A$ and $A = O(1)$ and the effective capillary number is small, the physical situation is that of a deep fluid pool filling much of the cylinder with a thin film coating the top, and again a Landau–Levich–Derjaguin argument may be utilized to predict the film thickness at small effective capillary numbers, despite the moderate filling fraction. As usual, the curvature between the thin film and the pool must be matched, and the features of the deep pool are determined by a static calculation.

An important question to be addressed is when the solutions we have described are observed experimentally. There are two issues to be considered. First, there are the restrictions we have placed on the parameters $\mathscr{R}, \lambda, \mathscr{B}$ and A (which have been documented above). These restrictions are such that although it would be difficult to achieve all of these regimes with one particular cylinder, given the limited variation of surface tension that is possible, each regime can in principle be achieved experimentally using a cylinder of an appropriate size.

Secondly, we must consider when the solutions are stable. Benjamin *et al.* (1993) proved stability of the two-dimensional solutions under perturbations dependent on θ alone when $2.00 \leqslant \lambda \leqslant 4.86$ in the absence of surface tension and first-order gravity, and Hosoi & Mahadevan (1999) performed numerical calculations which showed that the two-dimensional solutions were stable to three-dimensional perturbations when the Reynolds number is sufficiently small in the presence of surface tension. It has not been possible to prove stability of the other solutions analytically. However, in each case numerical solutions have been obtained by allowing the time-dependent equation

to evolve to a steady state, and the two-dimensional profiles described above have been obtained. Therefore it appears that these profiles are at least numerically stable under perturbations dependent on θ alone, but the numerics do not imply stability under perturbations which also depend on the axial coordinate. Experimental observations by Benjamin *et al.* (1993) and by Thoroddsen & Mahadevan (1997) reveal the existence of many different classes of space- and time-dependent states, including those with axial variations and periodic temporal dependence. Nevertheless, the work of Benjamin *et al.* includes observations of two-dimensional steady states when $0.357 < \lambda < 0.667$, which we would expect to be the approximately uniform films that are described in Appendix D, when $2.86 < \lambda < 5$ which we expect to be the solutions with regions of shape variation described in § 4 and by Tirumkudulu & Acrivos (2001), and when $\lambda \gtrsim 5$ which we expect to be of the form described in § 3 when the effective capillary number is small and of the form described by Tirumkudulu & Acrivos (2001) when the effective capillary number is large. The upper limit of λ in the experiments was not given. When $0.667 < \lambda < 2.86$ many different steady and time-dependent flows with axial variations were observed.

Many questions remain about the surprisingly complex behaviour of this system. Areas of possible interest in future research include analysis of the effects of inertia in the presence of surface tension, which has been demonstrated numerically to produce three-dimensional steady fingers by Hosoi & Mahadevan (1999), and further analytical and numerical investigation of the time-dependent instabilities which have been observed experimentally.

We thank J. Gordillo for helpful discussions, H.-C. Chang for useful comments and A. Acrivos for constructive criticisms that improved the presentation. We gratefully acknowledge the support of the Army Research Office (DAAG 55-97-1-0114) and of PPG Industries.

Appendix A. Governing equations

The dimensional steady Navier–Stokes equations for an incompressible two-dimensional flow in cylindrical coordinates are

$$\frac{1}{r}\frac{\partial}{\partial r}(ru_r) + \frac{1}{r}\frac{\partial u_\theta}{\partial \theta} = 0, \tag{A 1a}$$

$$\rho\left(u_r\frac{\partial u_r}{\partial r} + \frac{u_\theta}{r}\frac{\partial u_r}{\partial \theta} - \frac{u_\theta^2}{r}\right) = -\frac{\partial p}{\partial r} + \mu\left(\mathscr{D}^2 u_r - \frac{2}{r^2}\frac{\partial u_\theta}{\partial \theta}\right) + \rho g\cos\theta, \tag{A 1b}$$

$$\rho\left(u_r\frac{\partial u_\theta}{\partial r} + \frac{u_\theta}{r}\frac{\partial u_\theta}{\partial \theta} + \frac{u_r u_\theta}{r}\right) = -\frac{1}{r}\frac{\partial p}{\partial \theta} + \mu\left(\mathscr{D}^2 u_\theta + \frac{2}{r^2}\frac{\partial u_r}{\partial \theta}\right) - \rho g\sin\theta, \tag{A 1c}$$

where

$$\mathscr{D}^2 f = \frac{\partial}{\partial r}\left(\frac{1}{r}\frac{\partial}{\partial r}(rf)\right) + \frac{1}{r^2}\frac{\partial^2 f}{\partial \theta^2}. \tag{A 2}$$

We seek the velocity field $(u_r(r, \theta), u_\theta(r, \theta))$ and pressure field $p(r, \theta)$ which satisfy these equations and the boundary conditions (2.2*a*, *b*). Since

$$\boldsymbol{n} = \left(1 + \frac{h'(\theta)^2}{r^2}\right)^{-1/2}\left(\boldsymbol{e}_r + \frac{h'(\theta)}{r}\boldsymbol{e}_\theta\right), \quad \boldsymbol{t} = \left(1 + \frac{h'(\theta)^2}{r^2}\right)^{-1/2}\left(-\frac{h'(\theta)}{r}\boldsymbol{e}_r + \boldsymbol{e}_\theta\right), \tag{A 3}$$

the free-surface boundary conditions (2.2*b*) at $r = R - h(\theta)$ are

$$\boldsymbol{t}\cdot\boldsymbol{T}\cdot\boldsymbol{n} = 0 \Rightarrow \left(1 - \frac{h'(\theta)^2}{r^2}\right)T_{r\theta} + \frac{h'(\theta)}{r}(T_{\theta\theta} - T_{rr}) = 0 \tag{A 4a}$$

$$\boldsymbol{n}\cdot\boldsymbol{T}\cdot\boldsymbol{n} = 0 \Rightarrow T_{rr} + \frac{2h'(\theta)}{r}T_{r\theta} + \frac{h'(\theta)^2}{r^2}T_{\theta\theta} = -p_0 + \gamma\kappa, \tag{A 4b}$$

which correspond to

$$-\frac{h'(\theta)}{r}\frac{\partial u_r}{\partial r} + \frac{1}{2}\left(1 - \frac{h'(\theta)^2}{r^2}\right)\left[\frac{1}{r}\frac{\partial u_r}{\partial\theta} + r\frac{\partial}{\partial r}\left(\frac{u_\theta}{r}\right)\right] + \frac{h'(\theta)}{r}\left(\frac{1}{r}\frac{\partial u_\theta}{\partial\theta} + \frac{u_r}{r}\right) = 0, \tag{A 5a}$$

$$-p + \mu\left[\frac{\partial u_r}{\partial r} + \frac{h'(\theta)}{r}\left[\frac{1}{r}\frac{\partial u_r}{\partial\theta} + r\frac{\partial}{\partial r}\left(\frac{u_\theta}{r}\right)\right] + \frac{h'(\theta)^2}{r^2}\left(\frac{1}{r}\frac{\partial u_\theta}{\partial\theta} + \frac{u_r}{r}\right)\right] = -p_0 + \gamma\kappa. \tag{A 5b}$$

Non-dimensionalizing according to (2.4), the equations become

$$-\frac{\partial\tilde{u}_r}{\partial\tilde{r}} + \frac{A}{1 - A\tilde{r}}\tilde{u}_r + \frac{1}{1 - A\tilde{r}}\frac{\partial\tilde{u}_\theta}{\partial\theta} = 0, \tag{A 6a}$$

$$A^3\mathscr{R}\left(-A\tilde{u}_r\frac{\partial\tilde{u}_r}{\partial\tilde{r}} + \frac{A\tilde{u}_\theta}{1 - A\tilde{r}}\frac{\partial\tilde{u}_r}{\partial\theta} - \frac{\tilde{u}_\theta^2}{1 - A\tilde{r}}\right) = \frac{\partial\tilde{p}}{\partial\tilde{r}} + A^2\tilde{\mathscr{D}}^2\tilde{u}_r - \frac{2A^3}{(1 - A\tilde{r})^2}\frac{\partial\tilde{u}_\theta}{\partial\theta} + A\lambda\cos\theta, \tag{A 6b}$$

$$A^2\mathscr{R}\left(-\tilde{u}_r\frac{\partial\tilde{u}_\theta}{\partial\tilde{r}} + \frac{\tilde{u}_\theta}{1 - A\tilde{r}}\frac{\partial\tilde{u}_\theta}{\partial\theta} + \frac{A\tilde{u}_r\tilde{u}_\theta}{1 - A\tilde{r}}\right) = -\frac{1}{1 - A\tilde{r}}\frac{\partial\tilde{p}}{\partial\theta} + \tilde{\mathscr{D}}^2\tilde{u}_\theta + \frac{2A^3}{(1 - A\tilde{r})^2}\frac{\partial\tilde{u}_r}{\partial\theta} - \lambda\sin\theta, \tag{A 6c}$$

where

$$\tilde{\mathscr{D}}^2 f = \frac{\partial^2 f}{\partial\tilde{r}^2} - \frac{A}{1 - A\tilde{r}}\frac{\partial f}{\partial\tilde{r}} - \frac{A^2}{(1 - A\tilde{r})^2}f + \frac{A^2}{(1 - A\tilde{r})^2}\frac{\partial^2 f}{\partial\theta^2}. \tag{A7}$$

The boundary conditions and the integral constraint on the fluid volume are

$$\boldsymbol{u} = \boldsymbol{e}_\theta \quad \text{at } \tilde{r} = 0, \tag{A 8a}$$

$$\frac{A^2\tilde{h}'(\theta)}{1 - A\tilde{r}}\frac{\partial\tilde{u}_r}{\partial\tilde{r}} + \frac{1}{2}\left(1 - \frac{A^2\tilde{h}'(\theta)^2}{(1 - A\tilde{r})^2}\right)\left[\frac{A^2}{(1 - A\tilde{r})}\frac{\partial\tilde{u}_r}{\partial\theta} - (1 - A\tilde{r})\frac{\partial}{\partial\tilde{r}}\left(\frac{\tilde{u}_\theta}{(1 - A\tilde{r})}\right)\right] + \frac{A^2\tilde{h}'(\theta)}{(1 - A\tilde{r})}\left(\frac{1}{(1 - A\tilde{r})}\frac{\partial\tilde{u}_\theta}{\partial\theta} + \frac{A\tilde{u}_r}{(1 - A\tilde{r})}\right) = 0, \quad \text{at } \tilde{r} = \tilde{h}, \tag{A 8b}$$

$$-\tilde{p} - A^2\frac{\partial\tilde{u}_r}{\partial\tilde{r}} + \frac{A^2\tilde{h}'(\theta)}{1 - A\tilde{r}}\left[\frac{A^2}{1 - A\tilde{r}}\frac{\partial\tilde{u}_r}{\partial\theta} - (1 - A\tilde{r})\frac{\partial}{\partial\tilde{r}}\left(\frac{\tilde{u}_\theta}{\tilde{r}}\right)\right] + \frac{A^4\tilde{h}'(\theta)^2}{(1 - A\tilde{r})^2}\left(\frac{1}{1 - A\tilde{r}}\frac{\partial\tilde{u}_\theta}{\partial\theta} + \frac{A\tilde{u}_r}{1 - A\tilde{r}}\right) = -p_0 + \lambda\mathscr{B}^{-1}\tilde{\kappa} \quad \text{at } \tilde{r} = \tilde{h}, \tag{A 8c}$$

$$\int_0^{2\pi}\left[\tilde{h}(\theta) - \frac{A\tilde{h}(\theta)^2}{2}\right]\mathrm{d}\theta = \pi. \tag{A 8d}$$

One limit is $A^2\mathscr{R} = O(1)$, in which case the effects of centripetal forces may be studied (Ruschak & Scriven 1976). However, we assume that $A^2\mathscr{R} \ll 1$ and neglect the inertial terms, focusing instead on the leading-order and first-order ($O(A)$) effects of viscous, gravitational and surface tension forces. The equations and boundary conditions (A 6), (A 8), with $O(A^2\mathscr{R})$ and $O(A^2)$ terms neglected, are those given in (2.6), (2.7) and are the basis of our study.

Appendix B. Numerics

The numerical program used is that developed by Hosoi & Mahadevan (1999). We consider the interface to be time-dependent $h(\theta, t)$ and the time-dependent non-dimensional flux conservation equation is

$$(1 - Ah)\frac{\partial h(\theta,\ t)}{\partial t} + \frac{\partial q(\theta,\ t)}{\partial \theta} = 0, \tag{B 1}$$

where time has been scaled by Ω^{-1} and

$$q = h - \tfrac{1}{3}\lambda h^3 \sin\theta + \tfrac{1}{3}\lambda\mathscr{B}^{-1}h^3\frac{\partial \kappa}{\partial \theta} - A\left[\tfrac{1}{2}h^2 - \tfrac{1}{2}\lambda h^4 \sin\theta + \tfrac{1}{3}\lambda h^3 h' \cos\theta + \tfrac{1}{6}\lambda\mathscr{B}^{-1}h^4\frac{\partial \kappa}{\partial \theta}\right], \tag{B 2}$$

and κ is given by (2.8). The inclusion of time dependence on time scales comparable with and larger than Ω^{-1} can be studied with these equations, as described in the body of the text and Appendix A, so long as the effective Reynolds number $A^2\rho\Omega R^2/\mu$ is small, which is assumed to hold here. Equations (B 1) and (B 2) are allowed to evolve to a steady state, using an implicit time differencing scheme with time step Δt chosen by a 'step-doubling' algorithm. Newton's method with three iterations is used at each time step.

The first-order error in Δt is eliminated via extrapolation in the following way. The solution $h(\theta, t)$ is evolved forward in time in two different ways, first using one time step of size Δt to give a solution we shall denote by $h_1(\theta, t + \Delta t)$ and, secondly, using two time steps of size $\Delta t/2$ to give a different solution $h_2(\theta, t + \Delta t)$. The first-order error in Δt is eliminated by taking the extrapolated state to be

$$h_{\text{extrapolated}}(\theta, t + \Delta t) = 2h_2(\theta, t + \Delta t) - h_1(\theta, t + \Delta t). \tag{B 3}$$

A non-uniform mesh is used to resolve the solution $h(\theta,\ t)$ and the nonlinear terms are averaged before they are differentiated. Initial conditions for the solutions with $\lambda < 2$ and $2 < \lambda < 5$ were

$$h(\theta, t = 0) = 0.5 + 0.4\sin\theta, \tag{B 4}$$

and for those with $\lambda > 5$ were

$$h(\theta, t = 0) = 0.5 + 0.4\cos\theta. \tag{B 5}$$

Since all derivatives of these continuously differentiable functions are themselves continuously differentiable, all terms in equation (B 1) were initially continuous and remained so.

A number of other initial conditions were also used to probe for additional possible steady-state solutions since it is not clear that the nonlinear flux equation (2.13) has a unique solution. However, we always found that for the same values of the parameters

λ, $\lambda\mathscr{B}^{-1}$ and A reported here, different initial conditions always resulted in the same steady state.

Appendix C. $\lambda \gtrsim 5$, high effective capillary number

In this appendix we establish the constraints on the Bond number $\mathscr{B}$ and the filling fraction A for the high effective capillary number solution, and the limit $\lambda \gtrsim 5$, presented recently by Tirumkudulu & Acrivos (2001). Like the two solutions valid for low effective capillary numbers when $\lambda \gtrsim 5$ presented in § 3, the solution in this limit has a pool of fluid that sits at the bottom of the cylinder as viscous forces are too weak relative to gravitational forces to pull the fluid up from the bottom. It also has a film which is pulled out of the pool and which coats the sides and top of the cylinder; however, unlike the thin films in the solutions of § 3, in this case gravitational forces are important in the film and surface tension is unimportant in setting the film thickness. The film solution bears a close resemblance to the films generated by solutions valid in the limit $2 \lesssim \lambda \lesssim 5$. In order to derive the limits of validity, we describe the asymptotic scaling of the pool region and the transition region where the film is pulled out of the pool.

The pool solution is identical to that described in § 3.1 for the low effective capillary number solution in the limit $\mathscr{B}^{-3/5} \ll A \ll 1$. The thin film is generated by a balance between viscous and leading-order gravity forces. The flux equation (2.13) reduces to a cubic equation for the interface height in this region since first-order gravity and surface tension effects are both negligible. Since the pool and film have different asymptotic scales, there is additionally a transition region where the film is withdrawn from the pool where gradients are large and the first-order gravity term is important. Using these ideas, we can calculate asymptotic scalings for the interface thickness and the scale of θ over which variations occur in the pool, the transition region and the thin film.

The arguments used to derive the solution in the pool region in § 3.1 apply here and therefore the results of (3.1) are valid. In the thin film, a balance of the viscous and gravity terms leads to the scaling

$$h_{\text{film}} \approx \frac{1}{(\lambda\theta^*)^{1/2}}, \tag{C 1}$$

where $\theta^* \ll 1$ denotes the angle at which the film is withdrawn from the pool and we have again used the small-angle approximation for $\sin\theta$. From the pool balance, $\theta^* \approx \Delta\theta \approx A^{1/3}$ so that $h_{\text{film}} \approx \lambda^{-1/2}A^{-1/6}$. Variations in θ in the film occur over a scale $O(1)$.

In the transition region, the scale of θ-variations ℓ is set by the requirement that there is a smooth transition between the pool and the film. Viscous, gravity and first-order gravity terms are all important and therefore

$$h_{\text{film}} \approx \lambda h_{\text{film}}^3 \theta^* \approx A\lambda \frac{h_{\text{film}}^4}{\ell} \qquad \Rightarrow \ell \approx \frac{A^{1/2}}{\lambda^{1/2}}. \tag{C 2}$$

Since $\ell \approx A^{1/2}/\lambda^{1/2} \ll 1$, the curvature may be large and it is necessary to verify that surface tension is negligible, as has been assumed. Comparing the size of the surface tension term to the size of the viscous and gravitational terms in the transition region gives rise to the condition

$$\lambda\mathscr{B}^{-1}\frac{H^4}{\ell^3} \ll \frac{1}{\lambda^{1/2}A^{1/6}} \quad \Rightarrow \frac{A^2\mathscr{B}}{\lambda} \gg 1. \tag{C 3}$$

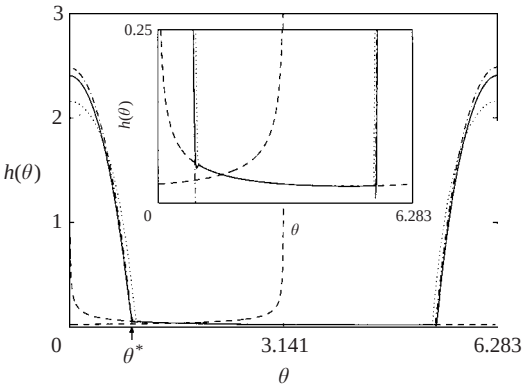

FIGURE 19. Plot of the two positive roots to the flux equation (2.13) for $q = 2/3\sqrt{\lambda}$ in the absence of first-order gravity and surface tension effects, given by (C 4*a*, *b*) (dashed lines), the theoretical prediction (3.1) using $\theta^* = 0.917$ (dot-dash lines), and two numerical solutions with $\lambda = 600$, $\mathscr{B} = 15000$, $A = 0.2$ (solid and dotted lines). The solid line indicates the solution obtained when both surface tension and first-order gravity effects are included; the dotted line is the solution generated by neglecting surface tension effects but including first-order gravity effects, using the methods described by Tirumkudulu & Acrivos (2001). Since $A^2\mathscr{B}/\lambda = 1$, this solution is in the crossover region between the two asymptotic limits $A^2\mathscr{B}/\lambda \ll 1$ and $A^2\mathscr{B}/\lambda \gg 1$. The inset shows the film region on a larger scale.

Including the contribution of the third derivative in the surface tension term leads to a condition for validity of this solution which differs from the condition determined by Tirumkudulu & Acrivos (2001). Overall, the constraints on the high effective capillary number solution valid when $\lambda \gtrsim 5$ are $\mathscr{B}^{-3/5} \ll A \ll 1$ and $A^2\mathscr{B}/\lambda \gg 1$, as indicated in the body of the text (see table 2). In the notation of Tirumkudulu & Acrivos (2001), these constraints are $F/\alpha = \beta \gtrsim 2.2$, $\mathscr{C} \gg F^{4/3}/\beta^2 = \alpha^2/F^{2/3}$ and $\mathscr{C}/F \gg 1$.

As observed by Tirumkudulu & Acrivos (2001), the flux $q = 2/(3\sqrt{\lambda}) + O(A)$ as in the limit $2 \leqslant \lambda \leqslant 5$. We observe that using this information, the interface height $h(\theta)$ is known analytically to within $O(A)$ in both the pool region and the film region. The pool shape is given by (3.1) for $2\pi - \theta^* < \theta < \theta^*$ and the film thickness is given by the formula of O'Brien & Gath (1988):

$$h(\theta) = \frac{2}{\sqrt{\lambda \sin\theta}} \cos\left(\frac{\cos^{-1}(-\sqrt{\sin\theta})}{3}\right) \quad \text{when } \theta^* < \theta < \frac{\pi}{2}, \tag{C 4a}$$

$$h(\theta) = \frac{2}{\sqrt{\lambda \sin\theta}} \cos\left(\frac{\cos^{-1}(-\sqrt{\sin\theta}) - 2\pi}{3}\right) \quad \text{when } \frac{\pi}{2} < \theta < 2\pi - \theta^*. \tag{C 4b}$$

In this formula, the principle value of the inverse cosine function is used. At the points where the film is pulled out of the pool and where it re-enters, the transition between the solutions in the two regions is made smooth by the first-order gravity term. In figure 19, a numerical solution of equation (2.13), a second numerical solution generated from a flux equation in which surface tension is neglected but first-order gravity effects are retained (Tirumkudulu & Acrivos 2001), and the theoretical predictions for the film region (C 4*a*, *b*) and in pool region are plotted. The theoretical solution in the pool region is the function $h(\theta)$ given in equation (3.1), but since $\theta^* \approx 1$ in this case and the analytical prediction for θ^* given in (3.1) is valid only when $\theta^* \ll 1$, here we obtain θ^* by numerically integrating the expression for $h(\theta)$ in the pool and determining θ^* such that the integral constraint $\int_{-\theta^*}^{\theta^*} h(\theta)\,\mathrm{d}\theta \approx \pi$ is

satisfied. This yields a value $\theta^* = 0.917$. There is reasonable agreement between the theoretical prediction and the numerical solutions in the pool region and in the film region.

This approach presented by Tirumkudulu & Acrivos (2001) for high effective capillary numbers, described in this appendix by starting with the lubrication equation (2.13), is valid when rotation is slow in the sense that $\lambda \gtrsim 5$ but is sufficiently fast that the effective capillary number is large. When rotation is slow in the sense that the effective capillary number is small, the solutions are as described in § 3.

Appendix D. $\lambda \ll 1$

When the cylinder is spinning sufficiently fast, though not so fast that inertial effects are important, the viscous forces are large in comparison to the gravitational forces and $\lambda \lesssim 2$. The fluid is easily pulled up from the bottom of the cylinder, and hence we would expect an approximately uniform film coating the inside of the cylinder for any value of the surface tension. The shape of the interface and the flux q can be expressed in the form of a power series in λ and the higher-order corrections to the leading-order uniform interface shape and flux can be determined. Part of this work was undertaken by Ruschak & Scriven (1976), and we summarize their results and add further analysis below.

D. 1. $A < \lambda < 1$: *gravitational perturbation*

Following Ruschak & Scriven (1976) we consider $\lambda \ll 1$ and seek a power series representation of the solution $h(\theta)$. We write

$$h(\theta, \lambda) = \sum_{k=0}^{\infty} \lambda^k h_k(\theta), \quad q = \sum_{k=0}^{\infty} \lambda^k q_k, \tag{D 1}$$

where $h_k(\theta)$ are functions and q_k are constants which are determined uniquely by imposing periodic boundary conditions and the integral condition

$$\frac{1}{2\pi} \int_0^{2\pi} h_k(\theta)\, \mathrm{d}\theta = \begin{cases} \pi, & k = 0 \\ 0, & k > 0. \end{cases} \tag{D 2}$$

Such a representation should be valid when $A < \lambda \ll 1$. Substituting (D 2) into (2.13) and neglecting terms $O(A,\ A\lambda,\ A\lambda\mathscr{B}^{-1})$, we find that the leading- and first-order terms are

$$h(\theta, \lambda) = \tfrac{1}{2} + \tfrac{1}{24}\lambda \sin\theta + O(\lambda^2), \qquad q = \tfrac{1}{2} + O(\lambda^2), \tag{D 3}$$

as first determined by Ruschak & Scriven (1976). The first two terms are independent of surface tension, which affects only terms $O(\lambda^2)$.

We continue to $O(\lambda^2)$ in order to determine an analytical approximation to the reduction of the flux observed in figure 14. Surface tension does affect the second-order solution and it is necessary to make an assumption about the magnitude of the parameter $\lambda\mathscr{B}^{-1}$. When $\lambda\mathscr{B}^{-1} \gtrsim O(1)$, the second-order term is

$$h_2(\theta) = q_2 + \tfrac{1}{192} + a\cos 2\theta + b \sin 2\theta, \tag{D 4}$$

where the constants a, b satisfy the equations

$$\lambda\mathscr{B}^{-1} a + 4b = 0, \tag{D 5a}$$

$$4a - \lambda\mathscr{B}^{-1} b = -\tfrac{1}{48}. \tag{D 5b}$$

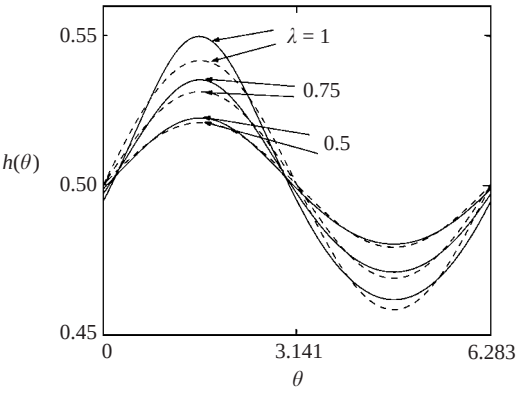

FIGURE 20. Plot of numerical solution to full equations and analytical solution with $\mathscr{B} = 10$, $A = 0.1$. The solid lines represent the numerical solution to the full equation (2.13) and the dashed lines represent the theoretical results from (D 4) taking values of a and b as given by (D 6*a*).

This leads to solutions

$$a = -\frac{1}{12(16 + (\lambda\mathscr{B}^{-1})^2)}, \quad b = \frac{\lambda\mathscr{B}^{-1}}{48(16 + (\lambda\mathscr{B}^{-1})^2)}, \tag{D 6a}$$

$$q = \tfrac{1}{2} - \tfrac{1}{192}\lambda^2 + O(\lambda^3). \tag{D 6b}$$

The approximate theoretical solution (D 4) and the full numerical solution are plotted in figure 20 for $\lambda = 0.5, 0.75, 1$. This illustrates that while for $\lambda = 0.5$ the approximation is good, there is some error when $\lambda = 1$. Higher-order terms may also be found, thereby giving better approximations to the reduction in the flux. However, the accuracy obtained just using the first correction term is reasonable and when $\lambda = 2$ the values of the two different theoretical estimates of the flux are $1/2 - \lambda^2/192 = 0.479$ and $2/3\sqrt{\lambda} = 0.471$.

Benjamin *et al.* (1993) found numerical solutions for the flux as a function of the rotation rate Ω in the zero surface tension case. The asymptotic behaviour they observe is $q = O(1)$ as $\lambda \to 0$ in accordance with our result (D 3). A comparison of equation (D 6) and our numerical results with zero surface tension and without the first-order gravity term is shown in figure 14(*a*).

We can now predict the flux for a wide range of λ using the prediction from this appendix when $A < \lambda \lesssim 2$ and that from § 3 when $2 \lesssim \lambda$.

REFERENCES

BALMER, R. T. 1970 The hygrocyst – a stability phenomenon in continuum mechanics. *Nature* **227**, 600–601.

BENJAMIN, T. B., PRITCHARD, W. G. & TAVENER, S. J. 1993 Steady and unsteady flows of a highly viscous fluid inside a rotating horizontal cylinder. Preprint.

BERTOZZI, A. L., MUNCH, A. & SHEARER, M. 1999 Undercompressive shocks in thin film flows. *Physica* D **134**, 431–464.

BRETHERTON, F. P. 1961 The motion of long bubbles in tubes. *J. Fluid Mech.* **10**, 166–188.

DUFFY, B. R. & WILSON, S. K. 1999 Thin film and curtain flows on the outside of a horizontal rotating cylinder. *J. Fluid Mech.* **394**, 29–49.

DERJAGUIN, B. 1943 Thickness of liquid layer adhering to walls of vessels on their emptying and the theory of photo- and motion-picture film coating. *C. R.* (*Dokl.*) *Acade. Sci. URSS* **39**, 13–16.

Hansen, E. B. & Kelmanson, M. A. 1994 Steady, viscous, free-surface flow on a rotating cylinder. *J. Fluid Mech.* **272**, 91–107.

Hinch, E. J. & Kelmanson, M. A. 2002 On the decay and drift of free-surface perturbations in viscous, thin-film flow exterior to a rotating cylinder. *Proc. R. Soc. Lond.* (to appear).

Hosoi, A. E. & Mahadevan, L. 1999 Axial instability of a free-surface front in a partially filled horizontal cylinder. *Phys. Fluids* **11**, 97–106.

Jensen, O. E. 1997 The thin liquid lining of a weakly curved cylindrical tube. *J. Fluid Mech.* **331**, 373–403.

Johnson, R. E. 1988 Steady-state coating flows inside a rotating horizontal cylinder. *J. Fluid Mech.* **190**, 321–342.

Karweit, M. J. & Corrsin, S. 1975 Observations of cellular patterns in a partially filled, horizontal cylinder. *Phys. Fluids* **18**, 111–112.

Kelmanson, M. A. 1995 Theoretical and experimental analyses of the maximum-supportable fluid load on a rotating cylinder. *J. Engng Maths* **29**, 271–285.

Landau, L. & Levich, B. 1942 Dragging of liquid by a plate. *Acta Physiochim. USSR* **17**, 42–54.

Melo, F. 1993 Localized states in a film-dragging experiment. *Phys. Rev.* E **48**, 2704–2712.

Moffatt, H. K. 1977 Behaviour of a viscous film on the outer surface of a rotating cylinder. *J. Méc.* **16**, 651–673.

Orr, F. M. & Scriven, L. E. 1978 Rimming flow: numerical simulation of steady, viscous, free-surface flow with surface tension. *J. Fluid Mech.* **84**, 145–165.

O'Brien, S. B. G. & Gath, E. G. 1988 The location of a shock in a rimming flow. *Phys. Fluids* **10**, 1040–1042.

Peterson, R. C., Jimack, P. K. & Kelmanson, M. A. 2001 On the stability of viscous free-surface flow supported by a rotating cylinder. *Proc. R. Soc. Lond.* A **457**, 1427–1445.

Preziosi, L. & Joseph, D. D. 1988 The run-off condition for coating and rimming flows. *J. Fluid Mech.* **187**, 99–113.

Pukhnachev, V. V. 1977 Motion of a liquid film on the surface of a rotating cylinder in a gravitational field. *Z. Prikl. Mekh. Tekh. Fiz.* **3**, 78–88; transl. *J. Appl. Mech. Tech. Phys.* **18**, 344–351.

Quéré, D. 1999 Fluid coating on a fiber. *Annu. Rev. Fluid Mech.* **31**, 347–384.

Rajagopalan, D., Phillips, R. J., Armstrong, R. C., Brown, R. A. & Bose, A. 1992 The influence of viscoelasticity on the existence of steady solutions in two-dimensional rimming flow. *J. Fluid Mech.* **235**, 611–642.

Ratulowski, J. & Chang, H. C. 1989 Transport of gas bubbles in capillaries. *Phys. Fluids* A **1**, 1642–1655.

Ruschak, K. J. & Scriven, L. E. 1976 Rimming flow of liquid in a rotating horizontal cylinder. *J. Fluid Mech.* **76**, 113–125.

Thoroddsen, S. T. & Mahadevan, L. 1997 Experimental studies of the instabilities in a partially filled horizontal rotating cylinder. *Exps. Fluids* **23**, 1–13.

Tirumkudulu, M. & Acrivos, A. 2001 Coating flows within a rotating horizontal cylinder: lubrication analysis, numerical computations and experimental measurements. *Phys. Fluids* **13**, 14–19.

Wilson, S. D. R. 1981 The drag-out problem in film coating theory. *J. Engng Maths* **16**, 209–221.

Wilson, S. D. R. & Jones, A. F. 1983 The entry of a falling film into a pool and the air-entrainment problem. *J. Fluid Mech.* **128**, 219–230.

Wilson, S. D. R. & Williams, J. 1997 The flow of a liquid film on the inside of a rotating cylinder, and some related problems. *Phys. Fluids* **9**, 2184–2190.

Wilson, S. K., Hunt, R. & Duffy, B. R. 2002 On the critical solutions in coating and rimming flow on a uniformly rotating horizontal cylinder. *Q. J. Mech. Appl. Maths* **55**, 357–383.